Expert Systems With Applications 232 (2023) 120655

Contents lists available at ScienceDirect

Expert Systems With Applications

journal homepage: www.elsevier.com/locate/eswa

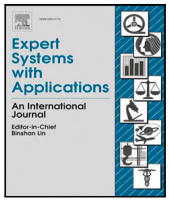

Review

Exploring the landscape of automatic cerebral microbleed detection: A comprehensive review of algorithms, current trends, and future challenges

Maria Ferlin [a,*], Zuzanna Klawikowska [a], Michał Grochowski [a], Małgorzata Grzywińska [b], Edyta Szurowska [b]

[a] Gdańsk University of Technology, 80-233 Gdańsk, Narutowicza 11/12, Poland
[b] Medical University of Gdańsk, 80-210 Gdańsk, Marii Skłodowskiej-Curie 3a, Poland

ARTICLE INFO

Keywords:
Classification
Detection
Segmentation
Cerebral microbleeds
CMB
Automatic diagnosis
Computer-aided diagnosis

ABSTRACT

This paper provides the first review to date which gathers, describes, and assesses, to the best of our knowledge, all available publications on automating cerebral microbleed (CMB) detection. It provides insights into the current state of the art and highlights the challenges and opportunities in this topic. By incorporating the best practices identified in this review, we established guidelines for the development of CMB detection systems. We are confident that these guidelines can serve as a foundation for further research.

CMB detection is a crucial but challenging task that can be laborious for radiologists. With the increasing popularity of magnetic resonance imaging (MRI), the ability to detect CMBs has improved, but there is still a need to automate this process to enhance its efficiency and accuracy. A high prevalence of CMBs is closely associated with cognitive dysfunction, diabetes, hypertension, an increased risk of stroke, and intracerebral hemorrhage. It is alarming to note that strokes, Alzheimer's disease, and Diabetes mellitus have secured their position as the second, seventh, and ninth most common causes of death worldwide, respectively. Moreover, CMBs are sometimes found in association with other pathologies and indicate a range of pathological processes in the cerebral vessels. Thus, it is essential to enhance the quality of diagnostics to facilitate prompt identification and treatment of these potentially life-threatening conditions.

In this paper, we aimed to systematize the existing knowledge and best practices in automatic CMB detection, from fundamental information about CMBs and MRI image data, through employed datasets and CMB detection and verification algorithms, to methods of result evaluation. This can serve as a starting point for future research and the development of a CMB detection system that is practically applicable in medicine, leading to enhanced patient treatment outcomes.

1. Introduction

Cerebral microbleeds (CMBs) are small, up to 10 mm in diameter, areas of bleeding in the brain. They can be defined, in terms of health and medicine, as small, homogeneous, hypointense foci well seen on T2*-weighted magnetic resonance imaging (MRI) sequences with the associated so-called 'blooming effect'. They are collections of blood degradation products (mainly hemosiderin) that can remain in macrophages for years, following a microhemorrhage (Cordonnier et al., 2007; Martinez-Ramirez et al., 2014; Shoamanesh et al., 2011; Werring, 2007). The 'blooming effect' takes place when the MRI overestimates the diameter of the microbleed (Greenberg et al., 2009).

The prevalence of microbleeds in the general population is estimated to be around 5% (Akoudad et al., 2015; Charidimou et al., 2018; Cordonnier et al., 2007). While many individuals with CMBs do not experience any related symptoms, their high occurrence is closely associated with cognitive dysfunction (Yakushiji et al., 2008), diabetes, hypertension, an increased risk of stroke, and intracerebral hemorrhage (Akoudad et al., 2015; Cordonnier et al., 2007, 2009). It is noteworthy that strokes, Alzheimer's disease, and Diabetes mellitus are collectively responsible for a significant number of deaths worldwide, claiming the lives of approximately 10 million people annually (World Health Organization, 2020). These diseases have secured their position as the second, seventh, and ninth most common causes of death worldwide, respectively. With the aging of the world's population and the rise of lifestyle-related health issues, it is expected that the incidence of these diseases and their associated complications will continue to

* Corresponding author.
E-mail addresses: maria.ferlin@pg.edu.pl (M. Ferlin), zuzanna.klawikowska@pg.edu.pl (Z. Klawikowska), michal.grochowski@pg.edu.pl (M. Grochowski), malgorzata.grzywinska@gumed.edu.pl (M. Grzywińska), eszurowska@gumed.edu.pl (E. Szurowska).

https://doi.org/10.1016/j.eswa.2023.120655
Received 17 March 2023; Received in revised form 18 May 2023; Accepted 30 May 2023
Available online 16 June 2023

increase in the foreseeable future. Moreover, CMBs are sometimes found in association with other pathologies (Bian et al., 2014) and can occur in every region of the brain (Fig. 1), indicating a range of pathological processes in the cerebral vessels (Martinez-Ramirez et al., 2014; Mazurek et al., 2018; Shams et al., 2016). Thus, it is crucial to improve the quality of diagnostics to facilitate prompt identification and treatment of these potentially life-threatening conditions.

CMB detection is a challenging task due to small size of the lesion compared to the whole image (Fig. 3). Moreover, there are many lesions that mimic the CMBs. The main CMB mimics include calcifications, flow voids in pial blood vessels, iron deposits, and deoxyhemoglobin Greenberg et al. (2009), which are described below. Both calcium and iron deposits may appear as small foci of low signal intensity on a T2*-weighted MRI. Flow voids caught in the cross-sections of cortical sulci can be distinguished from CMBs by their sulcal location, equal visibility on T2-weighted SE and GRE sequences, and linear structure when examined over contiguous slices, particularly evident at smaller slice thickness. The presence of paramagnetic deoxyhemoglobin in cerebral venules produces its own blooming effect, which requires the rater to rely on their tubular structure for differentiating them from CMBs. Metastatic melanoma in the brain can appear hypointense on T2*-weighted MRI and may mimic CMB. Other mimics, such as mineralization of the basal ganglia or diffuse axonal injury, for instance, can be excluded based on the appearance or clinical history.

From a medical standpoint, the number of detected cerebral microbleeds is significant information (Greenberg et al., 2009; Haller et al., 2018; Poels et al., 2011; Shams et al., 2015). Another valuable information is their location in the brain (Cordonnier et al., 2009; Cordonnier & van der Flier, 2011; Gregoire et al., 2009; Poels et al., 2012; Werring, 2004). Taking into account the medical information described above, marking CMBs using a bounding box is sufficient. Therefore, there is no need to perform a complex computational process, more specifically segmentation, in order to provide masks that indicate the contour of CMBs.

MRI technology has advanced to become a powerful tool for detecting cerebral microbleeds. MRI's high-resolution images allow radiologists to see even very small areas of bleeding. Unfortunately, assessing these images is a time-consuming process. Therefore, automated image processing assistance may offer a viable solution.

Various approaches have been proposed within last years. However, the issue is characterized by a marked degree of complexity and there is no consistency in the research. To the best of our knowledge, the results achieved so far are still not used in medical practice. Thereby, we acknowledged the necessity of organizing the current knowledge and most effective methodologies as a key factor in expediting the development of an applicable CMB detection system, which can be feasibly employed in the field of medicine.

Comparing the current research findings is a challenge due to the unavailability of publicly accessible datasets and the absence of standardized system evaluation metrics. By incorporating the best practices identified in this review, we established guidelines for the development of CMB detection systems. We are confident that these guidelines can serve as a foundation for the creation of new systems.

1.1. Review criteria

The aim of this research was to gather all previous works and achievements in the field of cerebral microbleed detection and propose the guidelines for development of a detection system. Regarding the lack of order in existing research and comparison ability we decided to collate different approaches and methods, in order to determine the current state of the art and provide a starting point for future studies. The detection of CMBs on MRI typically involves following certain instructions for radiologists (Charidimou et al., 2012, 2013; Charidimou & Werring, 2011; Cordonnier et al., 2007; Kaaouana et al., 2017; Tsushima et al., 2002). However, in this case, the emphasis lies on *automatization* since we aim to provide a set of guidelines for developers to design automatic detection CMB systems.

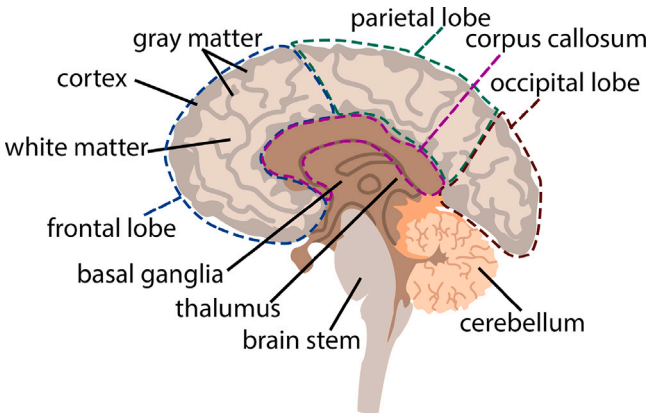

Fig. 1. Brain anatomy in the sagittal plane. In addition to the presented structures, the temporal lobe, the insula, and the external and internal capsules, which are not visible in this plane, are also important in the context of scales used to rate CMB. CMBs can be found in all structures indicated in the figure as well as in those mentioned above.

Firstly, a comprehensive literature review regarding automatic cerebral microbleed detection was done. We conducted a careful search for all papers connected with this topic in Google Scholar, IEEE Xplore, and Elsevier platforms, using key phrases: *automatic cerebral microbleed detection*, *automatic CMB detection*, *cerebral microbleed detection*. The next step was the search for related papers in the references of all gathered works. The literature review dates back to 2011 when, to the best of our knowledge, the first papers on automatic CMB detection were published.

Fig. 2 presents a schematic diagram of the structure of this research. The main information gathered from each paper referred to: database, pre-processing, methods used, proposed approach with the best or the most significant results, conclusions, and challenges. For the majority of modern methods, the key issue is the availability of datasets, therefore we decided to collate the information about all datasets used in this type of research in Section 2, which also introduces the issues of MRI and CMB characteristics and CMB rating. To maintain clarity of the paper, descriptions of particular algorithms are given in Section 3, while the exact approach leveraging from those algorithms is presented in Table 4. The algorithms described in Section 3 are divided into two main groups, referring to detection and verification of CMB candidates. Section 3.1 also presents different pre-processing algorithms that were used to prepare a dataset for training and testing. Then, all methods and algorithms that were used to solve this task are presented. The lack of standard metrics made evaluating results in the reported research challenging. This hindered comparison between existing approaches and assessing specific methods. To address this, we presented a range of metrics in Section 3.4, along with their features and dependencies. Section 4 provides a comprehensive assessment of all the presented research, followed by conclusions and challenges, both gathered during literature review and emerging from this analysis.

2. Data sources

In order to understand the task of cerebral microbleed detection, it is essential to understand the magnetic resonance imaging, acquisition process, and rating procedure. Therefore, we decided to introduce the process of MR image formation. Furthermore, the relevant sequences and rating scales were described. Finally, datasets used for cerebral microbleed detection were presented.

2.1. Magnetic resonance imaging sequences

Among the types of brain imaging the most common are CT (computed tomography) and MRI (magnetic resonance imaging). This paper

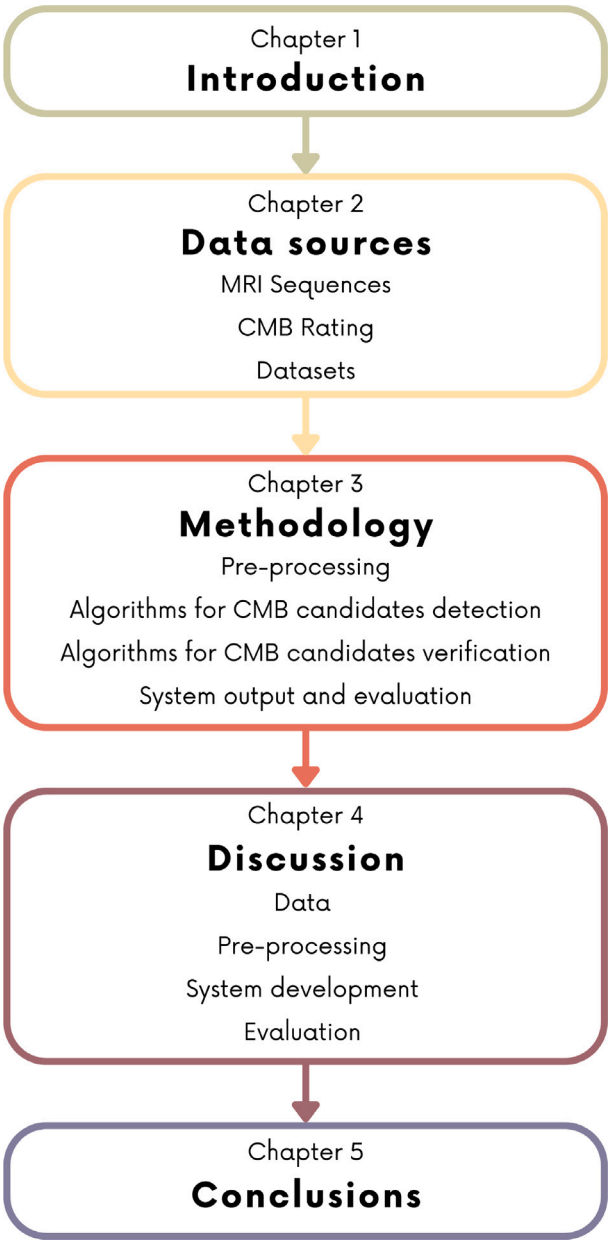

Fig. 2. Schematic diagram of the structure of the paper.

focuses on MRI since it is the preferred technique to detect CMBs. The main reason for this preference is that the density of the hemorrhage in CMBs, when observed via CT, declines rapidly over a few days, resulting in CMBs being indistinguishable from brain tissue after approximately 7 to 10 days. Haller et al. (2018). Consequently, the sensitivity of CT in CMB imaging is the highest within the first few days of their appearance. In contrast, on MR images, CMBs remain visible much longer than on CT.

MRI is the imaging technique that employs a combination of radio-frequency pulses and gradients in each sequence. There exist more than a hundred sequence types, with the acronyms being dependent on the manufacturer of the MRI machine. Regardless of the sequence name, the goal is to obtain the signal of a particular tissue, as quickly as possible, while limiting the artifacts and without altering the signal-to-noise ratio (Imaios, 2009).

Any imaging sequence must consist of three essential components. The first component is the radio frequency (RF) excitation pulse, which is required to generate the phenomenon of magnetic resonance. The second component comprises gradients for spatial encoding, whose arrangement will determine how the k-space is filled. Finally, the third component is signal reading, which combines different echo types that determine the type of contrast by varying influence of relaxation times. Additionally, further sequence parameters, such as repetition time or flip angle, must be chosen to achieve a trade-off between contrast, resolution, and speed (Currie et al., 2013).

There are three types of relaxation times, namely T1, T2, and T2* (Lipton, 2008). The term relaxation means that, once the RF pulse is turned off, the spins are relaxing back into their lowest energy state or to the equilibrium state, realigning with the axis of the magnetic field. T1 is called the longitudinal relaxation time, as it refers to the time needed for the spins to realign along the longitudinal (z)-axis. T2 is defined as the predicted time constant for the decay of transverse magnetization arising from natural interactions at the atomic or molecular level. However, in a real MR experiment, the transverse magnetization decays much faster than predicted by natural atomic and molecular mechanisms. This accelerated decay rate is denoted as T2*.

There are two main sequence families, depending on the type of echo recorded. The first family comprises Spin Echo (SE) sequences, which have two essential parameters: TR and TE. SE sequences consist of a series of events: 90° pulse; 180° rephasing pulse at half of echo time (TE) and signal reading at TE, repeated at each time interval TR (Repetition Time). During each repetition, the line of k-space is filled due to different phase encoding. The example of such sequence is FLuid Attenuation Inversion Recovery (FLAIR). The second family includes Gradient Echo (GE) sequences, during which the flip angle (FA) is usually below 90°, which decreases the amount of magnetization tipped into the transverse plane. In GE sequences, there is no 180° RF rephasing pulse. The example of this sequence is Susceptibility Weighted Imaging (SWI). Numerous variations have been developed within each of these families, mainly to increase the acquisition speed.

A **T1-weighted** (T1 W) sequence demonstrates differences in the T1 relaxation times of tissues. The T1-weighted image is consistent with the anatomy: gray matter is dark and white matter bright. Anatomical gray-white inversion is observed in **T2-weighted** (T2 W) images, in which gray matter is bright and white matter dark. It highlights differences in the T2 relaxation times of tissues. Another sequence is **FLAIR**, which removes signal from the cerebrospinal fluid (CSF) in the resulting image. Brain tissue in the FLAIR image appears similar to that in the T2 W image with gray matter brighter than white matter, but in this case, CSF is dark instead of bright. **SWI** is a 3D high-spatial-resolution fully velocity-corrected gradient-echo MRI sequence which takes advantage of the effect of both phase and magnitude. Fig. 4 shows the described sequences, while the data processing steps to obtain SWI are shown in Fig. 5.

As mentioned earlier, susceptibility-weighted sequences are named differently depending on the MRI vendor (Haller et al., 2021). For instance, Siemens has trademarked the term SWI, while GE Healthcare offers a sequence known as SWAN, and Philips Healthcare has suggested the name SWIp. Obtaining these sequences varies, due to licensing and patent issues (Nandigam & Scully, 2013). The dissimilarities between susceptibility-weighted sequences lie in the methods of combining the sequences. For instance, SWI employs phase and magnitude, whereas SWAN uses a weighted sum of longer TEs, which preserves T2* dephasing effects but also enhances the signal-to-noise ratio. Haller et al. (2021) and Hodel et al. (2012). However, regardless of the vendor, SWI-like sequences are most commonly used in CMB detection owing to their heightened sensitivity to this lesion compared to other sequences (Akiyama et al., 2009; Cheng et al., 2013; Nandigam et al., 2009; Park et al., 2009; Shams et al., 2015; Vernooij et al., 2008). SWI-like sequences are not only used in terms of automatic detection but also in everyday clinical practice. Another factor that influences the detectability of microbleeds is the strength of the magnetic

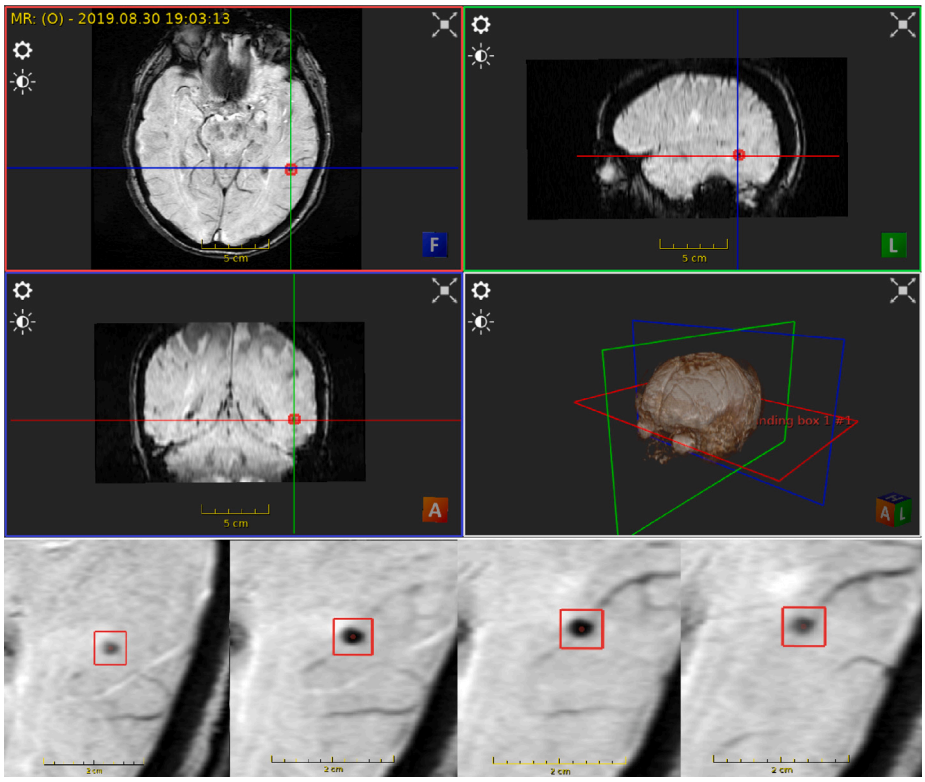

Fig. 3. Example of CMB. Upper images present the same microbleed in three planes, while bottom ones present sequence of adjacent slices fragments, in which the microbleed is visible (marked by red frame). Images acquired using ImFusion software.

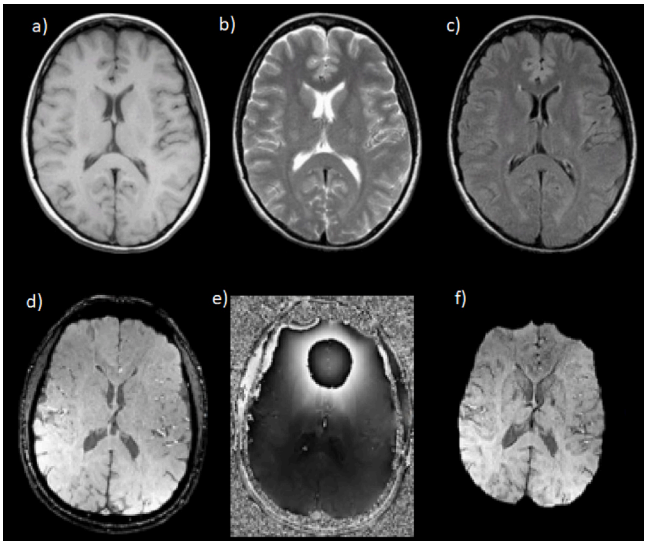

Fig. 4. Transverse brain plane. Sequences in first row (Preston, 2016): T1 W (a), T2 W (b), FLAIR (c); in second row (Liu et al., 2017) Magnitude (d), Phase (e), SWI (f).

field (de Bresser et al., 2013; Conijn et al., 2011; Nandigam et al., 2009; Scheid et al., 2007).

It is important to note that clinical image data is usually stored in the DICOM format. In contrast, for scientific analysis purposes, an alternative format called NIFTY is often preferred.

2.2. CMB rating

Technology that automates clinicians' work should be developed in accordance with clinical practice. Understanding the methods used to assess a disease is crucial to ensure that the results provided by the proposed system comply with established protocols. Clinicians utilize two scales to assess CMB: **Brain Observer Microbleed Scale** (BOMBS) (Cordonnier et al., 2009) and **Microbleed Anatomical Rating Scale** (MARS) (Gregoire et al., 2009), both of which were introduced in 2009. Table 1 outlines the evaluation categories for each scale.

Standardized CMB rating scales provide a consistent assessment methodology and enable straightforward and reliable quantification and categorization of CMBs even by individuals with different backgrounds or experiences. By providing a standardized approach, the reliability of the measurement is significantly enhanced.

Measurement reliability refers to the consistency or repeatability of the measurement. Low reliability indicates large differences in measurement during retesting. Poor reliability can compromise the reproducibility and interpretability of results, making it difficult to distinguish between individuals with and without specific medical conditions due to significant measurement error. There are two ways to determine observer reliability—inter- and intra-observer agreement.

Intra-observer agreement measures the level of agreement between two studies that utilize the same technique and are obtained by a single observer in the same subject (Filippi et al., 1995). **Inter-observer** agreement determines the degree of agreement between two studies that utilize the same technique and are obtained by two different observers in the same subject (Filippi et al., 1995).

The presence of CMBs plays a crucial role in accurately diagnosing various diseases, as the severity of these diseases can be determined by the number of CMBs present. However, it has been observed that many research institutions utilize their own distinctive methods to rate CMBs, and while their reliability based on intra- and inter-observer agreement is reported, the specific details of these methods are often not disclosed (Charidimou et al., 2012). To address this issue, it is essential to establish standardization and transparency in the methods used to rate CMBs, to ensure accurate and consistent diagnoses

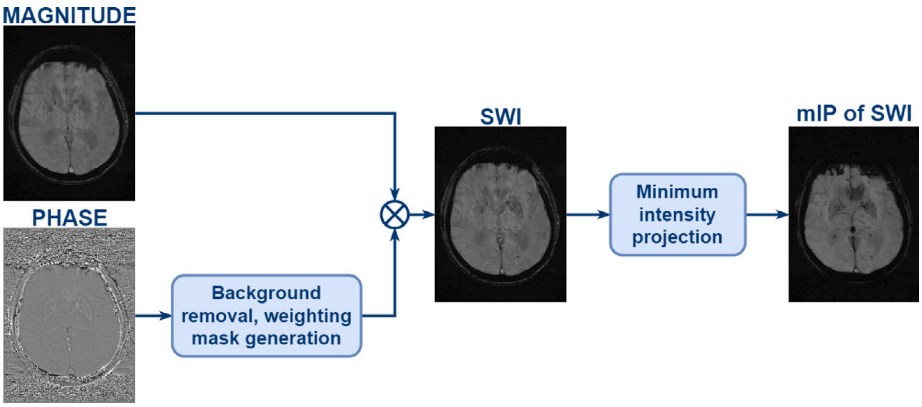

Fig. 5. Overview of data processing steps in SWI.

Table 1
CMBs evaluation categories according to rating scales.

BOMBS	MARS
1. certainty: (a) certain, (b) uncertain, 2. size: (a) <5 mm, (b) 5–10 mm, 3. side of the brain: (a) left, (b) right, 4. location (Fig. 1): (a) lobar: i. cortex/gray-white junction, ii. subcortical white matter, (b) deep: i. basal ganglia, ii. internal and external capsules, iii. thalamus, (c) posterior fossa: i. brain stem, ii. cerebellum.	1. appearance of the lesion: (a) definite, (b) possible, 2. side of the brain: (a) left, (b) right, 3. location (Fig. 1): (a) lobar: i. frontal, ii. parietal, iii. temporal, iv. occipital, v. insula, (b) deep: i. basal ganglia, ii. internal capsule, iii. external capsule, iv. thalamus, v. corpus callosum, vi. deep and periventricular white matter, (c) infratentorial: i. brain stem, ii. cerebellum.

across different research institutions. A uniform approach to rating CMBs would enable better comparisons between studies and facilitate a deeper understanding of the relationship between CMBs and various diseases, ultimately leading to improved clinical outcomes for patients.

2.3. Datasets

Studies regarding automatic CMB detection can be divided into two primary categories based on the source of the data used. The first category includes research that specifies the data source used for detecting CMBs, which is either an already existing dataset created for other purposes or a dataset prepared especially for automatic detection system development. The second category contains studies that do not specify the source of data used for CMB detection, and it is not clear how the data was obtained.

In research studies investigating CMBs, it is important to consider the potential effects of other comorbid conditions that may hamper proper detection and also have an impact on brain imaging. For instance, some conditions may increase the number of CMBs per patient, while in the case of TBI, the presence of a skull fracture can lead to artifacts in imaging studies. Hence, it is crucial to have knowledge of the other conditions that exist within the group from which the data was collected, apart from the presence of CMBs. The presence of other conditions for all patients in the dataset may be also a source of bias and limits the generalization ability of the system (Ferrer et al., 2023).

The medical conditions, in addition to the presence of CMB, of the patients whose imaging data were used in the studies reviewed are: Alzheimer's and elderly diseases (AD), Atherosclerosis (AS), Cerebral Amyloid Angiopathy (CAA), Cerebral Autosomal Dominant Arteriopathy with Subcortical Infarcts and Leukoencephalopathy (CADASIL), Cerebrovascular accident (CVA), Glioma Tumors (GT), Hemodialysis cases (HD), Intracerebral Haemorrhages (ICH), Second Manifestation of Arterial Disease (SMART), and Traumatic Brain Injury (TBI). However, not all researchers distinguish the additional condition. Table 2 presents a list of the reviewed studies, indicating whether the data source was specified and which other conditions were mentioned.

Clinicians rated the CMBs present in the images used in reviewed studies according to the MARS scale, BOMBS scale, scale based on these two, or an unspecified standard. Details related to the number of patients, image acquisition parameters, types of sequences, strength of magnetic field, and data availability are given in Table 3. Additional details about datasets are given in Table A.5 in Appendix. The abbreviations used in the table stand for: RES—resolution, TR—repetition time, TE—echo time, FA—flip angle, BW—bandwidth, IMS—image matrix size, ST—slice thickness, FOV—field of view, u - unknown dimension. Additional abbreviations appearing in the table are related to the classification by sequence type or dataset type and result from the cited reference's categorization.

Research that were not included in the table due to insufficient information are Bao et al. (2018), Doke et al. (2020), Fan et al. (2022),

Table 2
Categorization of papers by the source of the data and the condition on which the data focused.

Reference	Data source		Condition										
	Specified dataset	Unspecified dataset	AD	CADASIL	SMART	TBI	ICH	CAA	CVA	GT	HD	AS	CMB-only
Afzal et al. (2022)	–	✓	–	–	–	–	–	–	–	–	–	–	✓
Al-masni et al. (2020a)	✓	–	–	–	–	–	–	–	–	–	–	–	✓
Al-masni et al. (2020b)	✓	–	–	–	–	–	–	–	–	–	–	–	✓
Ateeq et al. (2018)	✓	–	–	–	–	–	–	–	–	–	–	–	✓
Bao et al. (2018)	–	✓	–	✓	–	–	–	–	–	–	–	–	–
Barnes et al. (2011)	✓	–	✓	–	–	–	–	–	–	–	–	–	–
Bian et al. (2013)	✓	–	–	–	–	–	–	–	–	✓	–	–	–
Chen et al. (2015)	✓	–	–	–	–	–	–	–	–	–	–	–	✓
Chen et al. (2017)	✓	–	–	–	–	–	–	–	–	–	–	–	✓
Chen et al. (2019)	✓	–	–	–	–	–	–	–	–	✓	–	–	–
Chesebro et al. (2021)	✓	–	✓	–	–	–	–	–	–	–	–	–	–
Doke et al. (2020)	–	✓	–	✓	–	–	–	–	–	–	–	–	–
Dou et al. (2016)	✓	–	–	–	–	–	–	–	–	–	–	–	✓
Dou et al. (2020)	✓	–	–	–	–	–	–	–	–	–	–	–	✓
Fan et al. (2022)	✓	–	–	–	–	–	–	–	–	–	–	–	✓
Fazlollahi et al. (2013)	✓	–	✓	–	–	–	–	–	–	–	–	–	–
Fazlollahi et al. (2014)	✓	–	✓	–	–	–	–	–	–	–	–	–	–
Fazlollahi et al. (2015)	✓	–	✓	–	–	–	–	–	–	–	–	–	–
Ferlin et al. (2021)	✓	–	–	–	–	–	–	–	–	–	–	–	✓
Ferrer et al. (2023)	✓	–	✓	–	–	–	–	–	✓	–	–	–	–
Ghafaryasl et al. (2012)	✓	–	✓	–	–	–	–	–	–	–	–	–	–
Gunter et al. (2018)	✓	–	✓	–	–	–	–	–	–	–	–	–	–
Gunter et al. (2022)	✓	–	✓	–	–	–	–	–	–	–	–	–	–
Hong, Cheng, Wang (2019)	✓	–	–	✓	–	–	–	–	–	–	–	–	–
Hong, Cheng, Zhang (2019)	✓	–	–	✓	–	–	–	–	–	–	–	–	–
Hong et al. (2020)	✓	–	–	✓	–	–	–	–	–	–	–	–	–
Kim et al. (2022)	✓	–	–	–	–	–	–	–	–	–	–	–	✓
Koschmieder et al. (2022)	✓	–	–	–	–	✓	–	–	–	–	–	–	–
Kuijf et al. (2011)	✓	–	–	–	✓	–	–	–	–	–	–	–	–
Kuijf et al. (2012)	✓	–	–	–	✓	–	–	–	–	–	–	–	–
Kuijf et al. (2013)	✓	–	✓	–	–	–	–	–	–	–	–	–	–
Lee et al. (2022)	✓	–	–	–	–	–	–	–	–	–	–	–	✓
Li et al. (2021)	✓	–	–	–	–	–	–	–	–	–	–	–	✓
Liu, Surapaneni et al. (2012)	✓	–	–	–	–	–	–	–	✓	–	–	–	–
Liu et al. (2019)	✓	–	–	–	–	✓	–	–	✓	–	✓	–	–
Liu et al. (2020)	✓	–	–	–	–	–	–	–	–	–	–	–	✓
Lu et al. (2017)	✓	–	–	–	–	–	–	–	–	–	–	–	✓
Lu et al. (2020)	–	✓	–	✓	–	–	–	–	–	–	–	–	–
Lu, Liu, Wang et al. (2021)	✓	–	–	✓	–	–	–	–	–	–	–	–	–
Lu, Nayak et al. (2021)	✓	–	–	✓	–	–	–	–	–	–	–	–	–
Lu, Yan et al. (2021)	–	✓	–	✓	–	–	–	–	–	–	–	–	–
Momeni et al. (2021)	✓	–	✓	–	–	–	–	–	–	–	–	–	–
Morrison et al. (2018)	✓	–	–	–	–	–	–	–	–	✓	–	–	–
Myung et al. (2021)	–	✓	–	–	–	–	–	–	–	–	–	–	✓
Nandigam et al. (2009)	✓	–	–	–	–	–	✓	✓	–	–	–	–	–
Nikseresht et al. (2022)	✓	–	✓	–	–	–	–	–	–	–	–	–	–
Roy et al. (2015)	–	✓	–	–	–	✓	–	–	–	–	–	–	–
Dou et al. (2015)	✓	–	–	–	–	–	–	–	✓	–	–	–	–
Rashid et al. (2021)	✓	–	–	–	–	–	–	–	–	–	–	✓	–
Sa-ngiem et al. (2019)	–	✓	–	–	–	–	–	–	–	–	–	–	✓
Seghier et al. (2011)	✓	–	–	–	–	–	–	–	✓	–	–	–	–
Standvoss et al. (2018)	–	✓	–	–	–	✓	–	–	–	–	–	–	–
Stanley and Franklin (2022a)	✓	–	–	–	–	–	–	–	–	–	–	–	✓
Stanley and Franklin (2022b)	✓	–	–	–	–	–	–	–	–	–	–	–	✓
Sundaresan et al. (2022)	✓	–	–	–	–	–	✓	–	✓	–	–	–	✓
Suwalska et al. (2022)	✓	–	–	–	–	–	–	–	–	–	–	–	✓
Tajudin et al. (2017)	–	✓	–	–	–	–	–	–	–	–	–	–	✓
Tao and Cloutie (2018)	–	✓	–	✓	–	–	–	–	–	–	–	–	–
van den Heuvel et al. (2015)	–	✓	–	–	–	✓	–	–	–	–	–	–	–
van den Heuvel et al. (2016)	–	✓	–	–	–	✓	–	–	–	–	–	–	–
Vieira (2023)	✓	–	–	–	–	–	–	–	–	–	–	–	✓
Wang et al. (2017)	–	✓	–	✓	–	–	–	–	–	–	–	–	–
Wang et al. (2019)	–	✓	–	✓	–	–	–	–	–	–	–	–	–
Wang et al. (2020)	–	✓	–	✓	–	–	–	–	–	–	–	–	–
Zhang et al. (2016)	✓	–	–	✓	–	–	–	–	–	–	–	–	–
Zhang, Hou et al. (2018)	✓	–	–	✓	–	–	–	–	–	–	–	–	–
Zhang, Zhang et al. (2018)	✓	–	–	✓	–	–	–	–	–	–	–	–	–

Gunter et al. (2022, 2018), Lu et al. (2017, 2020), Lu, Yan et al. (2021), Nikseresht et al. (2022), Standvoss et al. (2018), Suwalska et al. (2022), Tajudin et al. (2017) and Tao and Cloutie (2018). They contained limited information, for instance, only about the number of patients or the type of sequence.

3. Methodology

A comprehensive analysis of past works regarding cerebral microbleeds detection has led to the proposal of a generalized pipeline of such system. The majority of works can be divided into three stages:

Table 3
Comparison of dataset acquisition parameters used in the reviewed approaches sorted by dataset size.

Reference	# of subject/# of CMB	RES [mm^2]	ST [mm]	IMS [voxels]	FOV [mm^3\mm^2\ mm]	Sequences	β [T]	Public availability
Kuijf et al. (2011)	2/4	0.35 × 0.35	0.3	–	–	T2 ∗ W	7	On request
Barnes et al. (2011)	6/26	0.5 × 1	2	512 × 320 × 48	–	Fully flow-compensated 3 DGRE	1.5	–
Hong, Cheng, Wang (2019), Hong, Cheng, Zhang (2019), Hong et al. (2020)	10/–	0.5 × 0.5	2	364 × 448 × 48	–	SWI	3	–
Bian et al. (2013) and Morrison et al. (2018)	15/420	0.5 × 0.5	2	u × u × 40	240	T2 ∗ W	3	10 subjects
Kuijf et al. (2012)	18/54	0.35 × 0.35 T2 ∗ W, 0.66 × 0.66 T1W	0.3 T2 ∗ W, 0.7 T1W	–	–	T2 ∗ W, T1W turbo field echo	7	On request
Lu, Liu, Wang et al. (2021), Lu, Nayak et al. (2021), Wang et al. (2017, 2019), Zhang, Hou et al. (2018), Zhang et al. (2016) and Zhang, Zhang et al. (2018)	20/–	0.5 × 0.5	2	364 × 448 × 48	–	SWI	3	–
Afzal et al. (2022)	20/-	0.45 × 0.45	2	–	–	SWI	3	–
Chen et al. (2015) and Liu et al. (2020)	20/117	0.45 × 0.45	2	512 × 512 × 150	230 × 230	SWI	3	20 subjects
Vieira (2023)	20/170	0.45 × 0.45	2	512 × 512 × 150	230 × 230	SWI	3	20 subjects
Ateeq et al. (2018)	20/167	0.45 × 0.45	2	512 × 512 × 150	230 × 230	SWI	3	20 subjects
Rashid et al. (2021)	24/>157	1 × 1	1 T1WMP & T2W 1.5 SWI	256 × 256 × 176 T1WMP & T2W, 256 × 192 × 96 SWI	–	T1WMP, T2W, SWI	3	On request
Sa-ngiem et al. (2019)	26/–	–	3	u × u × 40–60	–	SWI	–	–
Roy et al. (2015)	26/404	0.45 × 0.45 SWI, 1 × 1 T1W-MPRAGE (magnetization prepared rapid gradient echo)	2 SWI, 1 T1W-MPRAGE	–	–	SWI, T1W-MPRAGE	3	–
Fazlollahi et al. (2013)	30/64	0.9 × 0.9	1.75	–	–	SWI	3	On request
Fazlollahi et al. (2014)	41/103	0.93 × 0.93 SWI, 1 × 1 T1W	1.75 SWI, 1.2 T1W	–	240 × 256 × 160 T1W	SWI, T1W	3	On request
Dou et al. (2015)	44/615	0.45 × 0.45	2	512 × 512 × 150	230 × 230	SWI	3	–
van den Heuvel et al. (2015, 2016)	51/627	0.98 × 0.98 SWI, 1 × 1 T1 MP-RAGE (T1MPR)	–	–	–	SWI, T1MPR	3	–
Li et al. (2021)	58/1301	–	5 T2F & T2WF, 2 SWAN-W	512 × 512 × u	240	T2F, SWAN-W, T2WF	3	–

(*continued on next page*)

Table 3 (*continued*).

Fazlollahi et al. (2015)	66/231	0.93 × 0.93 SWI, 1 × 1 T1W	1.75 SWI, 1.2 T1W	–	240 × 256 × 160 T1W	SWI, T1W	3	On request
Chesebro et al. (2021)	72/64	0.43 × 0.43 T2 ∗ W SWI, 0.43 × 0.43 T2 ∗ W GRE	1 T1W, 2 T2 ∗ W SWI, 1 T2 ∗ W GRE	–	256 × 200 T1W, 244 × 197 T2 ∗ W SWI, 220 × 181 T2 ∗ W GRE	T1W, T2 ∗ W SWI, T2 ∗ W GRE	3	On request
Kuijf et al. (2013)	72/148	0.96 × 0.96 T2 ∗ W & FLAIR, 1 × 1 T1W	3 T2 ∗ W & FLAIR, 1 T1W	–	–	T2 ∗ W, FLAIR, T1W turbo field echo	3	On request
Chen et al. (2019)	73/2835	0.5 × 0.5	1 SWI, 2 3DSPGR	512 × 512 × u	–	4-echo 3D TOF-SWI, 3DSPGR (3D Spoiled Gradient Recalled)	7	–
Seghier et al. (2011)	74/–	0.938 × 0.938	5	256 × 224 × u T2WFSE	240 × 180	T2WFSE, T2* GRE	1.5	On request
Koschmieder et al. (2022)	81/1761	1 × 1 T1 MP-RAGE 0.98 × 0.98 SWI	1	–	–	T1 MP-RAGE SWI	3	In future
Kim et al. (2022)	114/365	0.5 × 0.5	2	512 × 448 × 72	–	SWI, Phase	–	–
Lee et al. (2022)	116/367 DS1, 58/148 DS2	0.5 × 0.5	2 DS1, 3 DS2	–	256 × 224 × 144 DS1, 192 × 219 × 156 DS2	SWI	3	–
Al-masni et al. (2020a, 2020b)	72/188 HR, 107/572 LR	0.50 × 0.50 HR, 0.80 × 0.80 LR	2	512 × 448 × 72 HR, 288 × 252 × 72 LR	256 × 224 HR, 201 × 229 LR	SWI, Phase, Magnitude	3	No
Myung et al. (2021)	186/1716	0.63 × 0.63	2	–	220 × 198	3D Fast Field-Echo	3	–
Ferlin et al. (2021)	20/78 DS1, 179/760 DS2	0.45 × 0.45 DS1 0.50 × 0.50 DS2, 0.80 × 0.80 DS2	2	512 × 512 × 150 DS1 512 × 448 × 72 DS2, 288 × 252 × 72 DS2	230 × 230 DS1, 256 × 224 DS2, 201 × 229 DS2	SWI	3	20 subjects
Momeni et al. (2021)	214/235	0.93 × 0.93 SWI, 1 × 1 T1W	1.75 SWI, 1.2 T1W	-	240 × 256 × 160 T1W	SWI, T1W	3	On request
Liu et al. (2019)	220/1011	0.45-0.53 × 0.57-1.05 1.5T, 0.50–0.54 × 0.50-1.07 3T	2-2.65 1.5T, 2/2.3 3T	512 × 304-448 × 56/60 1.5T, 448-512 × 322-416 × 6/128 3T	–	–	1.5/3	On request
Ferrer et al. (2023)	148/– DS1, 20/– DS2, 62/– DS3	0.93 × 0.93 DS1, 0.45 × 0.45 DS2, 0.2-1 × 0.2-1 DS3	1.75 DS1, 1 DS2, 1-6 DS3	512 × 512 × 150 DS2	230 × 230 DS2	SWI	3 DS1 & DS2, 1.5/3 DS3	On request DS1, 20 subjects DS2
Ghafaryasl et al. (2012)	237/631	0.5 × 0.5	1.6 T2 ∗ W, 0.8 GRE PDW	–	–	3D T2 ∗ W, GRE Proton-Density weighted	1.5	–
Sundaresan et al. (2022)	270/>505	0.9 × 0.8 T2*-GRE, 0.8 × 0.8 SWI	5 T2*-GRE, 3 SWI	640 × 640 × 25 T2*-GRE, 256 × 288 × 48 SWI	–	T2*-GRE, SWI	–/3	On request
Dou et al. (2016)	320/1149	0.45 × 0.45	2	512 × 512 × 150	230 × 230	SWI	3	20 subjects
Stanley and Franklin (2022b)	320/1149	0.45 × 0.45	2	512 × 512 × 150	230 × 230	SWI	3	–
Stanley and Franklin (2022a)	320/1149 SWI 179/760 SVS	0.45 × 0.45 SWI	2	512 × 512 × 150 SWI	230 × 230 SWI	SWI	3	–

Pre-processing, *CMB Candidates Detection* and *CMB Candidates Verification*. Therefore, we decided to describe the methodology with the regard of such division. The overall idea is presented in Fig. 6. All the methods and algorithms available within each stage are first described

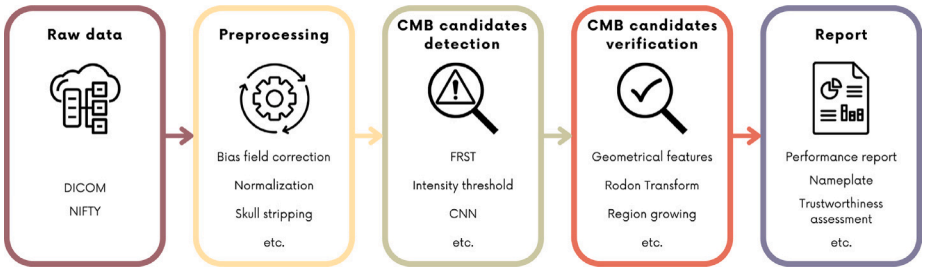

Fig. 6. Pipeline of a typical CMB detection approach.

as single transform that can be applied. Their further synthesis into a complete approach along with the paper in which it was used are in Table 4.

3.1. Pre-processing

Preparing data through pre-processing is a crucial phase in system synthesis, since it has a significant influence on the overall system's performance.

It is important to understand that the phrase *raw data* does not necessarily indicate that data were not pre-processed by MRI software. From the CMB detection system's perspective, raw data are those provided by the MRI. Nevertheless, there are numerous MRI device suppliers that develop their own operating systems and carry out diverse operations on a specific scan before delivering the final image. Therefore, it is crucial to know how the data has been processed thus far and determine what additional enhancements can be made to fulfill the requirements of the system.

The most popular types of operations performed on raw data are presented below along with some examples illustrated in Fig. 7. The first group of operations focuses on removing artifacts and unnecessary information.

Bias field correction is the operation that reduces negative influence of the bias field, which is an undesired artifact in most MRI images, especially old ones. It can also be called **intensity inhomogeneity correction**. The most commonly known techniques include N3 Bias Correction (Sled et al., 1998) and its successor N4ITK/N4 (Tustison et al., 2010), FSL FAST (Zhang et al., 2001) or reconstruction Syngo MR B17 provided by the manufacturer. Nevertheless, there are also other methods for bias field correction (Lupo et al., 2009; Song et al., 2017). This operation was applied by Fazlollahi et al. (2015, 2014), Ghafaryasl et al. (2012), Liu et al. (2019), Lu et al. (2020), Momeni et al. (2021), Rashid et al. (2021), Roy et al. (2015), Sundaresan et al. (2022), van den Heuvel et al. (2015, 2016) and Zhang et al. (2016).

Skull stripping also known as **brain extraction** is an operation of removing the skull and background from the image, leaving only the brain. There are plenty of algorithms for performing this task: Brain Extraction Tool (BET) (Smith, 2002), BrainSuite (Shattuck & Leahy, 2002), HD-BET (Lee et al., 2022) and others (Carass et al., 2011, 2007). Brain extraction was applied in Afzal et al. (2022), Al-masni et al. (2020a, 2020b), Ateeq et al. (2018), Barnes et al. (2011), Bian et al. (2013), Chen et al. (2019), Chesebro et al. (2021), Fazlollahi et al. (2014), Ghafaryasl et al. (2012), Kim et al. (2022), Koschmieder et al. (2022), Kuijf et al. (2011), Lee et al. (2022), Morrison et al. (2018), Myung et al. (2021), Nikseresht et al. (2022), Roy et al. (2015), Sundaresan et al. (2022), Suwalska et al. (2022) and van den Heuvel et al. (2015, 2016).

Normalization is a typical operation of rescaling the pixel values into range (0, 1) or (−1, 1). This enables bias reduction in the next stages of system synthesis. It was applied by Barnes et al. (2011), Bian et al. (2013), Chen et al. (2015), Dou et al. (2015), Fan et al. (2022), Fazlollahi et al. (2015, 2013, 2014), Ferlin et al. (2021), Kim et al. (2022), Koschmieder et al. (2022), Kuijf et al. (2013, 2011, 2012), Lee et al. (2022), Liu et al. (2019), Nikseresht et al. (2022), Rashid et al. (2021), Seghier et al. (2011), Stanley and Franklin (2022a) and van den Heuvel et al. (2015).

Standardization is an equally common operation as normalization and involves subtraction of mean value of pixels and division by the standard deviation of them. It was claimed to be used in Fan et al. (2022), Ferlin et al. (2021), Kuijf et al. (2013, 2011, 2012) and Suwalska et al. (2022).

Mask generation is a broad term given the fact different types of masks might be generated in the process. The most common one is a binary mask that might be generated using Statistical Parametric Mapping Toolbox (Ashburner et al., 2021), Fuzzy c-means clustering algorithm (FCCA), or morphological operations (Seghier et al., 2008; Soille, 2004). Further, there are typically neurological masks, such as the cerebrovascular fluid (CSF) mask, gray-white matter (GWM) mask, and white-matter (WM) mask. Additionally, some medical segmentation dedicated algorithms were developed, such as MimSeg (Binczyk et al., 2017). The masks were generated in Bian et al. (2013), Chen et al. (2019), Chesebro et al. (2021), Fazlollahi et al. (2015, 2013, 2014), Gunter et al. (2018), Hong et al. (2020), Kuijf et al. (2013, 2011, 2012), Liu et al. (2020), Sa-ngiem et al. (2019), Seghier et al. (2011), Stanley and Franklin (2022a), Suwalska et al. (2022) and van den Heuvel et al. (2015, 2016).

Further image generation involves using images provided by the MRI device to make a new image consisting of more information. For instance, an SWI sequence is generated from the Magnitude and Phase sequences. These days, it is the standard sequence generated by the scanner. Furthermore, the SWI data might be processed using (Li et al., 2014) for phase enhancement, like in Roy et al. (2015) Similarly, T2*-weighted images are nowadays provided by the MRI scanner, but in the past, they had to be obtained from PD-weighted images using, for example, Elastix Tool (Klein et al., 2010). It was performed, for example, in Ghafaryasl et al. (2012), Liu et al. (2019) and Chen et al. (2019). A QSM image can be generated using Morphology Enabled Dipol Inversion (MEDI) (Liu, Liu et al., 2012), like in Rashid et al. (2021).

Slice merging can also be considered as a new image creation, which involves the concatenation of adjacent slices to provide 3D information. MRI images are in grayscale, or, in other words, one-channel. Detection systems typically use full-color images with 3 channels, namely Red, Green, and Blue, known as RGB. To create an image containing spatial, three-dimensional information, these three channels can be used to generate an image by placing three adjacent single-channel slices from the MRI image. The concatenation of different sequences of corresponding slices might be done as well. However, in this case, it may be necessary to align the slices with each other, if there were different parameters of acquisition. This kind of operation was performed in Al-masni et al. (2020a, 2020b), Dou et al. (2016), Fan et al. (2022) and Ferlin et al. (2021).

Useful software to perform these operations is Neuroimaging Core (Patterson, 2019) involving Advanced Normalization Tools (ANT), FMRIB Software Library (FSL) (Ashburner & Friston, 2005; Jenkinson et al., 2002, 2012; Jenkinson & Smith, 2001) and Statistical Parametric

Mapping (SPM). The last software is also implemented in Ashburner et al. (2021) based on Penny et al. (2006).

Medical image pre-processing involves the application of various transformations that are commonly used in other fields where image pre-processing is necessary. These transformations comprise the second category of techniques employed in medical image pre-processing. It is noteworthy that medical data are highly sensitive to any transformation, after which significant information can be accidentally lost.

DICOM to JPG conversion is an excellent example of a lossy data conversion technique, which might influence further processing stages. It was done by Li et al. (2021). Although DICOM or NIFTY formats might be considered not developer-friendly, working on original image matrices should be a standard.

Resize is a common operation of changing image size. It is usually performed to obtain equal sizes of all images or to enlarge images to improve the visibility of the objects. It can also be forced by requirements of a method used in the *CMB Candidates Detection* stage. The images were resized in Barnes et al. (2011), Chesebro et al. (2021), Fan et al. (2022), Ferlin et al. (2021), Lee et al. (2022) and Liu et al. (2019).

Padding is an artificial size change by the addition of a black frame to obtain a desired image size without applying resize. It was utilized by Ferlin et al. (2021), Rashid et al. (2021) and Stanley and Franklin (2022a).

Image cut is a common operation performed to simplify the detection task. It involves image partitioning into smaller components and feeding them into the classifier. It might be performed using the sliding neighborhood processing (SNP) technique to produce smaller fragments of the original image. A lot of works utilized this method: Bao et al. (2018), Doke et al. (2020), Fan et al. (2022), Hong, Cheng, Wang (2019), Hong, Cheng, Zhang (2019), Hong et al. (2020), Kim et al. (2022), Lee et al. (2022), Lu, Liu, Wang et al. (2021), Lu et al. (2017), Lu, Nayak et al. (2021), Lu et al. (2020), Stanley and Franklin (2022a), Tao and Cloutie (2018), Wang et al. (2017, 2019), Zhang, Hou et al. (2018), Zhang et al. (2016) and Zhang, Zhang et al. (2018).

Rotation is a simple operation of changing image orientation. However, it can be a loss operation, and therefore a rotation with original intensity should be considered, like in Sundaresan et al. (2022), for instance by using—fslreorient2std tool (Jenkinson et al., 2012).

Inversion is the operation that consists of swapping intensity values in relation to the center of the intensity interval and it was performed by Fazlollahi et al. (2015).

Finally, there is **data augmentation**, which is not always considered a pre-processing technique, but rather a regularization one. However, it is sometimes performed at this stage and consists of image transformations, therefore it is placed in this section. It enhances a dataset, especially in case of a small amount of data by creating new, slightly modified, artificial images. There is a wide range of transformations, including those described above, along with blur, crop, etc. Buslaev et al. (2020), Mikolajczyk and Grochowski (2018) and Paszke et al. (2019). Augmentation was used in Afzal et al. (2022), Doke et al. (2020), Ferlin et al. (2021), Gunter et al. (2018), Li et al. (2021), Momeni et al. (2021), Myung et al. (2021), Rashid et al. (2021) and Standvoss et al. (2018).

3.2. Algorithms for CMB candidates detection

Over the years, a wide range of algorithms were used to detect cerebral microbleeds, starting from the simplest methods based on traditional image transformations to complex deep learning models.

3.2.1. Classical methods

In early works regarding CMBs detection, the candidates were extracted using predetermined features such as **intensity threshold** and **area size** (Ateeq et al., 2018; Barnes et al., 2011; Chen et al., 2015; Dou et al., 2015; Ghafaryasl et al., 2012). In the SWI sequence CMBs occur as low-intensity spheres, therefore applying a proper intensity threshold

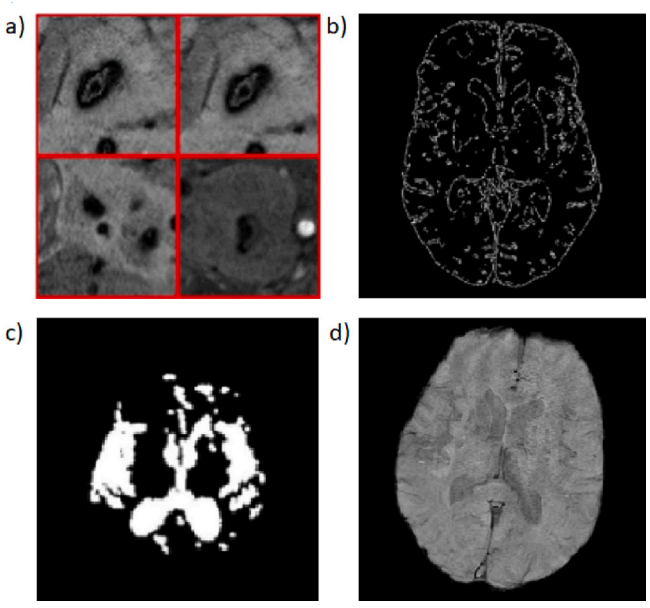

Fig. 7. Example of pre-processing operations: (a) sliding neighborhood processing (Hong et al., 2020), (b) Canny edge detection (Chesebro et al., 2021), (c) CSF mask (Myung et al., 2021) (d) brain extraction using BrainSuite software.

allows for **binary mask** generation. Occasionally, the authors also applied morphological operations such as **filtering**, **hole filling**, etc. Afzal et al. (2022), Ateeq et al. (2018) and Seghier et al. (2011). However, these kinds of operations were used at all the stages described in this paper, as they were also useful for *CMB candidates verification*. Over time, the detecting procedures evolved to include more complicated voxel features. The procedures contain methods such as **eigenvalues** in Sundaresan et al. (2022) – scalars associated with the given linear transformation, **line detection** in Fazlollahi et al. (2013) – defining the line where edge points are located, **Gaussian filter** in Sundaresan et al. (2022) and **Laplacian of Gaussian** operator in Fazlollahi et al. (2015, 2014) and Sundaresan et al. (2022), which highlight the rapid change of the image intensity, **Hough transform** in Chesebro et al. (2021) that enables shape detection by finding objects - local maxima, **Canny filter** in Chesebro et al. (2021) which enables edge detection **watershed transform** in Tajudin et al. (2017) - transforming images to gray-scale topographic like map, and distinguishing objects on the basis of its intensity value or **Frangi filters** in Sundaresan et al. (2022) - a dedicated filter enabling vessel distinction, or 3D gradient co-occurrence matrix (3D GCM) in Stanley and Franklin (2022a), which indicates the differences between intensity of two adjacent pixels, **region growing** (Revol-Muller et al., 2002) used in Roy et al. (2015) – inspection of the homogeneity of the considered pixel or voxel.

Simultaneously, the researchers began to use the Radial Symmetry Transform (RST) and its successor, Fast Radial Symmetry Transform (FRST) (Loy & Zelinsky, 2003). This algorithm deserves special attention since it is successfully used to this day (Bian et al., 2013; Chen et al., 2019; Kuijf et al., 2013, 2011, 2012; Liu et al., 2019; Morrison et al., 2018; Sundaresan et al., 2022). In this transform, a gradient of the image is computed, then the orientation and magnitude of each pixel are established. Next, using the above values, points of interest can be selected according to a specific formula. FRST was further developed so that it could be used in 3D space. However, despite its common use, it has some weaknesses. When applied to candidate detection, FRST generates a lot of false positives. Thus, there is a need for a third stage in the detection procedure.

The last distinguished classical algorithm is **random forest algorithm** (Breiman, 2001) which was used in van den Heuvel et al. (2015, 2016). Random forest is a black-box algorithm that consists of an

ensemble of classifiers that generate predictions. The algorithm utilizes a subset of the dataset to generate individual predictions, which are then combined through averaging to produce a final output value.

3.2.2. Artificial neural network-based methods

The development of artificial neural network (ANN) algorithms and their proven effectiveness to be a powerful tool for medical image analysis, has generated heightened interest in their utilization for CMB detection.

Two approaches to the use of ANN can be distinguished. The first one is to design a custom neural network. The second one uses a general-purpose pre-trained neural network.

In the first case, in the domain of CMB detection, various approaches were used, such as **artificial neural networks** (Wang, 2003) which consist of a sum of inputs multiplied by weights assigned in the training process, applied in Momeni et al. (2021) and Zhang, Zhang et al. (2018), **back-propagation neural networks** (BPNNs) (Buscema, 1998) that is ANNs extension with the information about the error, utilized in Tao and Cloutie (2018), **sparse auto-encoder** (SAE) (Lee et al., 2006) which is a neural network consisting of an encoder and decoder with the additional sparsity penalty algorithm, used in Zhang et al. (2016) and Zhang, Hou et al. (2018). An evolution of ANNs also includes **convolutional neural networks** (CNNs) (O'Shea & Nash, 2015). It is the most popular solution in case of automatic CMB detection (Doke et al., 2020; Gunter et al., 2018; Hong, Cheng, Wang, 2019; Hong et al., 2020; Lu, Liu, Wang et al., 2021; Lu et al., 2017; Lu, Nayak et al., 2021; Stanley & Franklin, 2022a; Wang et al., 2017). Standard CNN consists of a number of feed-forward convolutional layers, where the features are extracted by performing a convolution between input data and convolutional filters. Each convolution layer is followed by a non-linear activation function. Consecutive convolution layers are interspersed by pooling layers that extract the most important features. Then, there is a fully connected layer or alternative classifier that assigns a predicted class based on the previously extracted features. An interesting approach is a replacement of a fully-connected layer by Extreme Learning Machine (Huang et al., 2006), which is much more efficient (Lu, Liu, Wang et al., 2021).

Due to the fact that deep neural networks usually consist of millions of parameters and are hard to train due to hardware limitations, the second approach which uses a general-purpose pre-trained neural network is often used. It employs deep neural network architecture that has already been trained on a vast, unrelated dataset, often significantly different from the targeted one. Next, this architecture is adapted to the problem under consideration. This approach is known as transfer learning, which is the application of knowledge gained from completing one task to help solve a different problem. Additionally, transfer learning is a good method for dealing with slight dataset problems.

In the context of pre-trained general-purpose neural networks, various commonly-known architectures have been utilized, including AlexNet (Krizhevsky et al., 2012) in Sa-ngiem et al. (2019), ResNet50 (He et al., 2016) in Hong, Cheng, Zhang (2019), Faster-RCNN (Ren et al., 2015) in Ferlin et al. (2021), VGG (Simonyan & Zisserman, 2015) in Lu et al. (2020), U-Net (Ronneberger et al., 2015) in Rashid et al. (2021), YOLOv2 (Redmon & Farhadi, 2017) in Al-masni et al. (2020a) and Al-masni et al. (2020b), DenseNet 201 (Huang et al., 2018) in Wang et al. (2019) or SSD (Liu et al., 2016) in Li et al. (2021) with the modification of feature enhancement.

Occasionally, the detection task was replaced by classifying small fragments of an image using either CNN or ResNet50, as in Hong, Cheng, Wang (2019) and Hong, Cheng, Zhang (2019). Considering the main aim of this paper, the description of each network is omitted, as they are explained in detail in the mentioned papers. Nevertheless, the reader is strongly encouraged to get familiar with these architectures.

Recently, there has been an emergence of relatively new and promising deep learning architectures known as **3D convolutional neural networks** (3D CNNs). These models are still in their early stages and have not been fully explored, but their potential for applications in areas such as computer vision and medical imaging has garnered significant attention from researchers in the field. The fundamental concept behind 3D CNNs is similar to that of 2D CNNs, which involves performing convolutional operations. Nonetheless, in contrast to 2D CNNs, 3D CNNs operate on 3D data patches. Unfortunately, 3D CNNs require a significant amount of computational resources due to the increased dimensionality of the data. It is worth mentioning that 3D CNNs were utilized in Dou et al. (2016) and Standvoss et al. (2018), however, reported results do not exceed those performed on 2D images.

3.3. Algorithms for CMB candidates verification

CMB detection is a demanding process, and the presence of CMB mimics along with algorithmic errors can lead to a significant number of false positives. In order to mitigate this issue, a *CMB Candidates Verification* stage is sometimes implemented. Nonetheless, even with the implementation of this stage, certain approaches still have not managed to acquire satisfying quality.

In some cases, the process of false positive candidates elimination was performed manually by a radiologist (Barnes et al., 2011; Chen et al., 2019; Chesebro et al., 2021; Kuijf et al., 2013, 2011, 2012; Morrison et al., 2018). Although this kind of approach significantly reduced the time needed for one scan rating, it is a semi-automated one.

At the CMB candidates verification stage, most research identified a batch of predefined CMB features, such as intensity and size, or complex parameters of a single voxel, calculated in 2D or 3D spaces. Then, the features of CMBs together with the previously prepared fragments of images were passed to the classifier. A lot of classifiers were tested, including Support Vector Machine (SVM) (Chang & Lin, 2011) in Ateeq et al. (2018), Barnes et al. (2011), Chen et al. (2015) and Dou et al. (2015), linear criterion classifier (LDC) (Barnard & Casasent, 1989), quadratic discriminant classifier (QDC) (Tharwat, 2016), Parzen classifier (Jain & Ramaswami, 1988) in Ghafaryasl et al. (2012) and Random Forrest Classifier (RFC) (Breiman, 2001) in Fazlollahi et al. (2014) and Fazlollahi et al. (2015).

Moreover, there were also other methods to define CMB features to eliminate false positives, for instance, 2D CNN in Afzal et al. (2022) and Chen et al. (2015), 3D ISA network (Comon, 1995) in Dou et al. (2015), 3D Radon Transform (Averbuch & Shkolnisky, 2003) in Fazlollahi et al. (2015, 2014) or feed-forward feature selection (FFFS) (Luo et al., 2011) in Ghafaryasl et al. (2012). In some cases, thresholds of geometric features were set, and on this ground, the classification was performed (Bian et al., 2013, 2018; Chesebro et al., 2021; Roy et al., 2015; Sundaresan et al., 2022).

Another strategy at this stage was to use a previously generated CSF mask to distinguish a real CMB from vessels, and a WM mask to include the information about the location of potential microbleed (Bian et al., 2013; Chesebro et al., 2021; Myung et al., 2021). Some approaches utilized the advantage of a 3D CNN. It was typically performed to include 3D information, resulting in an FP reduction, after applying the 2D algorithm at the *Candidates detection stage* (Al-masni et al., 2020a, 2020b; Chen et al., 2019; Dou et al., 2016; Liu et al., 2019; Singh et al., 2020). Certain works also presented the use of the region-growing algorithm for CMB verification (Bian et al., 2013, 2018; van den Heuvel et al., 2016). In addition, there was an algorithm used to investigate the overlap between predictions from adjacent slices (Ferlin et al., 2021). It enabled not only the removal of false-positive predictions that were in fact a ground truth, although labeled in the adjacent slice but also helped find a real CMB that was detected in the adjacent slice in spite of the previous false-negative prediction.

3.4. System output and evaluation

To comprehensively validate the quality and robustness of the system, it is recommended to utilize several widely accepted metrics that provide complementary insight into various aspects of system performance.

A common oversight is not to include metrics that are complementary and provide a view of the system as a whole, not just a part of it. For instance, the sensitivity metric is insufficient alone, as it can be artificially inflated. It is necessary to provide the precision, or F1 score value, to properly interpret the sensitivity. In addition, the lack of a uniform way of result evaluation makes it impossible to compare approaches and effectively assess their effectiveness.

The evaluation should be performed on a separate dataset, or at least separate subjects, using, for instance, cross-validation to avoid randomness.

There are different metrics regarding the type of solved problem. For classification evaluation, the most widespread metrics are accuracy (1), precision (4), sensitivity/recall (2), and F1 score (5) which combines precision and sensitivity.

In the case of detection and segmentation, more detailed metrics are required given the fact that not only is a proper class important but so is the overlapped area of ground truth label and prediction. In that case, the average precision (7) metric is used, and it is calculated for different values of IoU (6).

The CMB detection task is known to produce a vast number of false-positive predictions. Therefore, two additional metrics were provided particularly for this problem, namely FPavg (8) and FPcmb (9).

The mentioned metrics are calculated as follows:

$$\text{accuracy} = \frac{TP + TN}{TP + TN + FP + FN} \tag{1}$$

$$\text{sensitivity} = \frac{TP}{TP + FN} \tag{2}$$

$$\text{specificity} = \frac{TN}{TN + FP} \tag{3}$$

$$\text{precision} = \frac{TP}{TP + FP} \tag{4}$$

$$\text{F1 score} = 2 \times \frac{\text{sensitivity} \times \text{precision}}{\text{sensitivity} + \text{precision}} \tag{5}$$

$$\text{IoU} = \frac{Overlaparea}{Unionarea} \tag{6}$$

$$\text{AP} = \int_0^1 p(r)\, dr \tag{7}$$

$$\text{FPavg} = \frac{FP}{n} \tag{8}$$

$$\text{FPcmb} = \frac{FP}{m} \tag{9}$$

where:

- TP — true positive – the number of actual CMBs detected;
- FP — false positive – the number of predicted CMBs that were not marked as CMB in ground truth;
- FN — false negative – the number of actual CMBs not detected;
- IoU — intersection over union;
- r — recall (sensitivity);
- $p(r)$ — precision as function of recall;
- n — the number of subjects (patients) in the test set;
- m — the number of CMBs in the test set.

Accuracy (ACC) (1) shows how the system deals with classification in general. A high score means that almost all labels have been properly assigned.

Sensitivity/recall (2), also known as true-positive rate (TPR), shows how the system deals with ground truth detection or classification. A high score means that almost all ground-true samples have been determined.

Specificity, also known as true-negative rate (TNR) (3), discloses the system's ability to recognize the negative class.

Precision (4), or positive predictive value (PPV), informs whether the prediction matches ground truth. A high score means that the system generates a small number of false positives.

F1 score (5) helps to check whether there is a balance between sensitivity and precision.

IoU (6) stands for Intersection over Union and shows the common area between prediction and ground truth. It is actually a special case of geometrically oriented Jaccard Index (Real & Vargas, 1996). The average precision (7) AP@0.5 represents the area under the precision–recall curve with IoU of 0.5, and it is used in detection and segmentation. There is also an AUC – area under the curve – metric. In the case of classification, it refers to the ROC curve - sensitivity as a function of $1 - specificity$.

FPavg (8) shows the average number of false-positive predictions per subject, while FPcmb (9) is the number of false-positive predictions per one ground truth sample. For example, when we have one subject with 5 ground truth CMBs and 1 false positive prediction. The FPavg will equal 1 and FPcmb will equal 0.2.

3.5. Comparison of existing approaches

Table 4 presents, in chronological order, multiple approaches regarding cerebral microbleed detection that took place in recent years. It can be observed that at first, the prevailing solutions were those based on traditional image processing techniques, and it was thereafter that the proposals based on machine learning algorithms took the lead. One can observe that these methods achieved considerably higher performance, both in terms of sensitivity and low false positive generation. Therefore, it can be assumed that the approach based on ML algorithms is more promising regarding practically applicable solutions. Alternatively, a combination of traditional and ML methods might be considered.

Regarding the pre-processing stage, there are several operations, such as bias field correction, skull stripping, and normalization, that should be done in the case of MRI analysis before feeding data into the system. Other transforms may also be used in particular cases, but they are not essential.

A substantial issue is related to selecting the type of solved problem, whether it should be classification, detection, or segmentation. A large part of solutions is based on cutting images into smaller fragments and their further classification. These approaches are reported to have a significantly better ability to distinguish CMB from its mimic. In the case of the detection process, great number of false-positive predictions are generated, which often forces the introduction of the second stage, namely false-positive reduction or predictions verification, as high false-positive generation is one of the main problems in CMB detection. Another challenge that can be overcome by using classification instead of detection is the size of the lesion. CMBs are small objects, which makes them difficult to detect in the original image. Dividing the image into sub-images enhances the visibility of these microbleeds.

Although the use of 3D CNN does not offer any significant improvement over 2D CNN, it is possible that a larger training dataset could enable the 3D CNN structure to be utilized more effectively, resulting in better performance. However, presently, opting for this solution is not encouraging due to the higher computational cost involved. Furthermore, it is evident that the research being reported frequently lacks certain metrics. While it may not be necessary to mention all indicators, it is vital to conduct a proper evaluation and present the results appropriately.

We wish to highlight that determining the optimal approach based on the data collected is challenging due to different datasets and shortcomings in reported metrics. However, there exist some promising

Table 4
Comparison of existing approaches[a]. The most promising ones are marked in bold.

Reference	Pre-processing	First stage	Second stage	TPR	PPV	F1	FPavg	FP/CMB	TNR	ACC
Kuijf et al. (2011)	SPM8, BET, normalization, standardization	3D RST	Manual inspection	–	–	–	5*	–	–	–
Seghier et al. (2011)	SPM8, normalization	CSF, GWM, CMBs, skull scalp, background img	Morphological operations (2 iterations)	Authors did not provide any metric, only the table of results for each case.						
Barnes et al. (2011)	Brain extraction, resize, normalization	Intensity histogram threshold	SVM, manual review	81.7	–	–	107.5*	5.4*	100	–
Ghafaryasl et al. (2012)	N3, Elastix, BET	Intensity and area threshold	FFFS →LDC, QDC, SVC, Parzen	90.9	–	–	4.1	1.8*	–	–
Kuijf et al. (2012)	SPM8, normalization, standardization	3D RST	Manual inspection	71.2	–	–	17.17	4.68*	–	–
Kuijf et al. (2013)	SPM8, normalization, standardization	3D RST	Manual inspection	87	–	–	45	–	–	–
Bian et al. (2013)	BET, ARC, mIP, normalization	FRST	Vessel mask screening, 3D region growing, geometric features	86.5	–	–	44.9	1.5*	–	–
Fazlollahi et al. (2013)	CSF, invertion, normalization, Gaussian blur	Multi-scale 1D line detection	Center detection → Hessian matrix	100	–	–	158.93*	–	99.9	–
Fazlollahi et al. (2014)	N4, CSF, skull-stripping, normalization, equalization, anisotropic diffusion	Multi-scale Laplacian of Gaussian	3D Rodon Transform → Hessian matrix, RFC	92.04	–	–	16.84	6.7*	–	–
Fazlollahi et al. (2015)	N4, CSF, inversion, normalization, equalization, anisotropic diffusion	Laplacian of Gaussian	3D Rodon Transform → Hessian matrix, RFC	87	–	–	27.1	–	–	–
Roy et al. (2015)	N4, skull stripping, phase enhancement	3D region growing	RST, WM mask, geometric features	85.7	–	–	–	–	99.5	–
Chen et al. (2015)	Normalization	Intensity threshold	CNN, 3D concatenation, SVM	89.13	56.16	68.91	6.4	–	–	–
Dou et al. (2015)	Normalization	Intensity threshold	ISA SVM	89.44	–	–	7.7	0.9	–	–
van den Heuvel et al. (2015)	FSL FLIRT, FSL FAST, N3, SPM12b, normalization	Voxel based features → RFC	–	90	–	–	–	1.3	–	–
Dou et al. (2016)	Slices merging	Hierarchical 3D CNN	3D CNN	93.16	44.31	60.06	2.74	–	–	
Zhang et al. (2016)	Reconstruction Syngo MR B17, SNP	SAE	–	93.20	–	–	–	–	93.25	93.22

(*continued on next page*)

solutions. In the case of classification, there are approaches proposed by Lu, Nayak et al. (2021), Lu, Yan et al. (2021), Stanley and Franklin (2022a, 2022b) and Wang et al. (2019) with the best ACC = 98.60%. Regarding detection, there are solutions presented by Ferlin et al. (2021) and Li et al. (2021) with F1 = 90.84%.

The aforementioned research stand out from for instance (Al-masni et al., 2020a, 2020b; Chesebro et al., 2021; Kim et al., 2022; Lee et al., 2022; Suwalska et al., 2022) in terms of balanced results. That means the first one provides similar values of all metrics, while the second one, although reporting satisfying sensitivity, suffers from a high false-positive prediction generation, which indicates low precision. Although Doke et al. (2020) and Hong et al. (2020) report high accuracy, the datasets used by them were insufficient in terms of patients number. Results reported in Ferlin et al. (2021), Li et al. (2021)

Table 4 (*continued*).

van den Heuvel et al. (2016)	FSL FLIRT, FSL FAST, N3, SPM12b	Voxel based features → RFC	Object classifier, growing-based algorithm	93	–	–	25.9	0.29	–	–
Lu et al. (2017)	Square window size	CNN	–	97.29	–	–	–	–	92.23	96.05
Wang et al. (2017)	SNP, discard borders, cost ratio	CNN + RAP	–	96.94	–	–	–	–	97.18	97.18
Tajudin et al. (2017)	–	Watershed transform, active contour (Chan-Vese)	–	Authors provided only mean square error MSE = 0.089 and peak signal to noise ratio PSNR = 34.5221						
Standvoss et al. (2018)	Augmentation, selective sampling	3D CNN, connected component analysis	–	87	–	–	16.75	2.5	–	–
Zhang, Hou et al. (2018)	SNP, discard borders, cost ratio	ANN	–	93.05	–	–	–	–	93.06	93.06
Zhang, Zhang et al. (2018)	SNP, discard borders	SAE-DNN	–	95.13	–	–	–	–	93.33	94.23
Ateeq et al. (2018)	BrainSuite	Intensity threshold, filtering, hole filling	SVM, QDA, ensemble classifier	93.7	–	–	56	5.3	–	–
Morrison et al. (2018)	BET	FRST	Region growing, geometric features, manual validation	86.7	–	–	44.9	1.5*	–	–
Bao et al. (2018)	SNP	Bayesian classifier	–	74.53	–	–	–	–	74.51	74.52
Tao and Cloutie (2018)	SNP	GA-BPNN	–	72.90	–	–	–	–	72.89	72.90
Gunter et al. (2018)	Intensity threshold, image cut, data augmentation	CNN	–	Authors provided only AUC = 98.5						
Liu et al. (2019)	N4, SWI generation, resize, normalization	3D FRST	3D CNN	95.80	70.90	81.49*	1.6	0.39	–	–
Chen et al. (2019)	ARC, BET, SWI generation, negative phase mask	FRST	Manual validation, 3D ResNet	94.69	71.98	81.79	11.58	–	–	–
Wang et al. (2019)	Sliding window	Dense-Net 201	–	**97.78**	**97.65**	–	–	–	**97.64**	**97.71**
Hong, Cheng, Zhang (2019)	SNP	ResNet50	–	95.71	–	–	–	–	99.21	97.46
Hong, Cheng, Wang (2019)	SNP	CNN	–	98.87	–	–	–	–	96.49	97.68
Sa-ngiem et al. (2019)	Intensity enhancement, binarization, morphological operations, geometrical features	AlexNet, brain area extraction	–	–	–	–	–	–	–	95.45

(*continued on next page*)

and Stanley and Franklin (2022a) were obtained for relatively big but different datasets, therefore they are hard to compare with each other. From mentioned proposals only some can be compared, as they used the same dataset—like (Lu, Nayak et al., 2021; Wang et al., 2019) .

Table 4 (*continued*).

Hong et al. (2020)	SNP, brain area enhancement	CNN	–	99.74	–	–	–	–	96.89	98.32
Doke et al. (2020)	Sliding window, augmentation	CNN	–	98.97	99.66	–	–	–	98.14	98.54
Liu et al. (2020)	Binarization. noise reduction	Fourier descriptor	–	85.2	3.2	–	69.5	–	–	–
Lu et al. (2020)	Reconstruction Syngo MR B17, SNP	VGG-ELM-BAC	–	93.08	–	–	–	–	87.12	90.00
Al-masni et al. (2020a, 2020b)	BET, slices merging	YOLOv2	3D-CNN	94.32	61.94	74.78	1.42	–	–	–
Rashid et al. (2021)	N4, QSM generation, padding, normalization, augmentation	U-Net	–	84	59	–	–	–	–	–
Chesebro et al. (2021)	BET, CSF mask, resize	Sobel filter, Hough transform	CSF filtering, 3D geometric filtering, manual validation	95.00	11.00	19.72	9.7	–	–	–
Myung et al. (2021)	BET augmentation	YOLO	CSF filtering	66.90	79.75	72.76	2.15	–	–	–
Li et al. (2021)	ANTs, JPG conversion, augmentation	SSD + FE	–	**90**	**79.7**	**84.54***	–	**0.23**	–	–
Ferlin et al. (2021)	Padding, resize, normalization, standardization, slices merging, annotations modification augmentation	Faster RCNN	Overlap between slices	**92.62**	**89.74**	**90.84**	**0.24**	–	–	–
Lu, Liu, Wang et al. (2021)	SNP	CNN + ELM + BA	–	92.93	–	–	–	–	83.35	88.56
Lu, Nayak et al. (2021)	SNP	CNN + EN	–	**98.27**	–	–	–	–	**98.93**	**98.60**
Momeni et al. (2021)	N4, augmentation, synthetic CMBs generation	ANN	–	18.6	9.2	–	3.6	–	99.4	96.8
Lu, Yan et al. (2021)	SNP	CNN	–	**98.18**	**98.54**	**98.36**	–	–	**98.60**	**98.39**
Afzal et al. (2022)	BrainSuite, augmentation	K-means clustering, geometrical features	Alex-Net	97.26	–	–	–	–	96.5	96.21

(*continued on next page*)

Nevertheless, the aforementioned meticulous and comprehensive analysis offers an opportunity to draw conclusions, outline the best practices, and identify the essential components of a reliable automated detection system for cerebral microbleeds that are included in Section 4 below.

4. Discussion

This section addresses the crucial aspects of an automated detection system for cerebral microbleeds that we deem significant. After a careful analysis of all the gathered scholars, we decided to present our thoughts and conclusions related to the most reasonable, meaningful, and, in our opinion, practical approaches to the problem being analyzed.

4.1. Data

As emphasized earlier, the importance of data cannot be diminished when it comes to the development and implementation of an automated detection system, particularly for a ML model. While traditional image processing methods may not require large amounts of data for training, it is still essential to have adequate dataset for system evaluation,

Table 4 (*continued*).

Stanley and Franklin (2022a)	Resize, contrast stretching, normalization, Gaussian Filter, histogram equalization, morphological operations, Sharr gradient, 3D GCM	1D CNN + LSTM	–	**98.76**	–	**98.78**	–	–	**97.21**	**98.24**
Sundaresan et al. (2022)	fslreorient2std, FSL FAST, BET	Frangi filters, FRST, intensity transformations, eigenvalues, Gaussian filter, Laplacian of Gaussian	Geometric features level threshold	91	–	–	–	–	81	86
Suwalska et al. (2022)	BET,	MiMSeg,	Filtration,	90	21.95	–	0.54	–	98.95	–
	standardization, gray-scale change	3D region growing,	geometric features, mask, CNN	91.5	48	–	1.92	–	95.2	–[b]
Koschmieder et al. (2022)	HD-BET, N4,	3D-FRST	CNN	87.7	–	–	6.9	1.51	–	–[c]
	normalization,	Segmentation CNN		91	–	–	5.5	1.27	–	–
	growing,		3D U-Net	92.2	–	–	3.4	1.08	–	–
Kim et al. (2022)	SWI generation, normalization, BET, slice interpolation, random crop/ sliding window	Faster R-CNN, U-Net	–	94.66	25.64	–	8.82	–	–	–
Nikseresht et al. (2022)	N4,	U-Net,	PCA,	58.23	18.70	–	5	–	–	–
	normalization, BET	Frangi filters, Hessian eigenvalue, mask,	ResNet18							
Lee et al. (2022)	BET, normalization, interpolation, crop, resize, augmentation	EfficientDet-D3, ensemble of three plane detection	–	96.05	76.76	–	0.88	–	–	–
				85.03	79.67	–	0.55	–	–	–[d]
Stanley and Franklin (2022b)	N4,	EEWMDC	ELM, CNN,	**97.11**	**97.31**	–	**3.5**	–	**97.24**	**98.06**[e]
	sharpening, FCCA, crop	feature extraction	SVM, CS, CO							
Fan et al. (2022)	Intensity scale, standardization, normalization, crop, resize, slice merging	3D U-Net	–	88.96*	80.9*	–	–	–	–	–
Gunter et al. (2022)	–	Resample, normalized cross-correlation,	ANN	95	–	–	0.6	–	–	–
Vieira (2023)		3D FCN	3D CNN with spatial pyramid pooling	96.94	95.48	–	9.0	–	–	–
Ferrer et al. (2023)	Augmentation	MultiResUNet	Ensemble of three plane detection	0.80	0.80		1.92			

[a]Data marked with * were not provided in original paper. Instead, they were calculated either by us or the Authors of other papers listed in Table 4, based on data provided in the original paper.

[b]Results achieved on additional validation dataset (see Table 3).

[c]Authors presented three alternative methods for the first and second stages. The pre-processing was shared.

[d]Results achieved on additional validation dataset (see Table 3).

[e]The best results achieved for ELM classifier.

as well as for the validation and testing phases. This is because the accuracy and effectiveness of the system depend on the quality and quantity of the data used for the training. Therefore, a varied and a broad dataset is necessary to ensure that the system can detect cerebral microbleeds effectively and efficiently in a wide range of conditions. By using a diverse dataset, the system can be trained to recognize different variations of cerebral microbleeds regardless of the MRI machine, leading to a more robust and reliable automated detection system.

In Section 2, the paper lists a range of datasets that were used in reviewed approaches to the automatic CMB detection. However, these datasets differ not only in their acquisition parameters but also in terms of the origin and medical history of the patients. Moreover, there were cases where the information about the used dataset is incomplete or inconsistent with the source article, for example Suwalska et al. (2022).

The diversity between datasets makes it extremely challenging to compare proposed approaches. Thus, standardization of the datasets descriptions is necessary. In our opinion, it is essential to provide information such as the origin of the data, its number, the acquisition parameters, the sequence type, and a thorough MRI rating procedure. At later stages, this could also enable verification of the datasets in terms of biases and identification of their source. Standardization of the datasets descriptions would facilitate the development of more robust and reliable automated detection systems for cerebral microbleeds and enable more accurate comparison between proposed approaches.

Moreover, some datasets have an insufficient number of subjects, as highlighted in studies such as Barnes et al. (2011) and Kuijf et al. (2011). In such cases, the tested subset may be not representative enough to validate the proposed approach and conclusions drawn. The system trained on such a narrowed dataset will reveal low generalization ability, as noted in van den Heuvel et al. (2016). To prevent over-fitting, it is crucial to have a large and diversified dataset. Advanced regularization techniques, as described in Lee et al. (2022) and Nusrat and Jang (2018), should also be applied to ensure optimal training of the automated detection system.

It is worth underlining that in case of classical methods the whole dataset may be used for testing purposes as the method itself does not require data for training process. In contrast, when we consider the machine-learning approaches most of available data is used for system synthesis, including training. Therefore, the test subset is significantly smaller and with relatively low number of samples the assessment of generalization ability might be limited.

An interesting approach to overcome the data shortage problem was proposed by Momeni et al. (2021) and Nikseresht et al. (2022). It consisted of synthetic microbleeds generation based on previously extracted CMB features. Another way to produce huge amounts of synthesized data is employing the Generative Adversarial Network (GAN) (Creswell et al., 2018). GAN is capable of generating novel images by utilizing the features automatically extracted from a pre-existing dataset comprising authentic objects. Nevertheless, it is worth noting that both of these approaches also require a considerable amount of data to initiate the process effectively. Although there is a possibility of generating biased data, both methods still show promise in expanding datasets along with other augmentation techniques.

To ensure impartial results, it is considered a good practice to use a completely unrelated dataset for testing when evaluating a system. In recent studies such as Ferlin et al. (2021), Lee et al. (2022), Momeni et al. (2021) and Suwalska et al. (2022) adoption of this approach can be observed. An *unrelated dataset* refers to data that has been acquired from a different MRI machine, from subjects with different origins and medical histories, and ranked by another rater. MRI examinations performed on various machines may have different parameters, making it important to synthesize a system that is resistant to features that should not directly impact prediction. The use of various datasets allows to evaluate the model's generalization ability. However, while using an unrelated dataset is desired, it is not always achievable in practice.

The limited availability of the datasets used in research is another constraint that hinders the comparison of different approaches. It is typical among researchers to either not share their data or share it in a restricted manner, as indicated in datasets comparison Table 3. This lack of transparency and openness in data sharing limits the potential for validation of the proposed approaches. To address this issue, we encourage open data sharing to promote reproducibility and transparency of scientific research.

Establishing a benchmark dataset could significantly accelerate the development in the addressed medical domain, despite the numerous legal restrictions on medical data sharing (Leming et al., 2022). This has already been demonstrated in the cases of brain glioma segmentation (Baid et al., 2021) and determining skeletal age (Halabi et al., 2019; Siegel, 2019).

Concluding, the dataset is the base of the computer-aided detection system. It should be as large and diversified as possible. Moreover, to provide transparency and comparison possibility, data should be publicly available and precisely in the paper—with all acquisition parameters.

4.2. Pre-processing

The pre-processing stage is also an important aspect to consider when it comes to synthesizing a system. As described in Section 3.1, there is a large number of possible operations that can be applied. They should be adjusted considering the original image properties and designed system requirements. Typically, we can divide approaches into two groups—those where pre-processing is limited to necessary operations like normalization and those where it plays an important role in the detection such as SNP (see Table 4). Nevertheless, any image transformations should be thought-out and justified. Bias field correction is a commonly used method in MRI pre-processing, as it can restore important information. Using dedicated tools for skull stripping is also preferred over simply removing part of the image, as demonstrated in Wang et al. (2017), Zhang, Hou et al. (2018) and Zhang, Zhang et al. (2018). However, even with dedicated pre-processing techniques, images passed to the system may still be unintentionally deformed or partial. It is important to take precautions to prevent valuable data loss. Therefore, any operations that modify the image's size should be performed without content loss for instance in Sundaresan et al. (2022).

4.3. System development

When it comes to system design, we came to the conclusion that there are several issues that should be addressed.

Firstly, the MRI data is given in the three-dimensional space. Regardless of the algorithm employed, there is a stage in which information from the third dimension must be used. Especially in the case of detecting cerebral microbleeds, spatial dependencies play a crucial role in distinguishing the CMBs from their most common mimics, which are blood vessels (Al-masni et al., 2020a; Bian et al., 2013; Chen et al., 2019, 2015; Chesebro et al., 2021; Dou et al., 2016; Fan et al., 2022; Fazlollahi et al., 2014; Ferlin et al., 2021; Koschmieder et al., 2022; Lee et al., 2022; Liu et al., 2019; Suwalska et al., 2022). While the vessels can be distinguished based on spatial information, the other CMB mimic, such as calcification, has a similar shape in the 3D space. In such cases, utilizing additional MRI sequences, apart from SWI, can be advantageous for identifying these mimics (Al-masni et al., 2020a). The existing approaches can be categorized into three groups in terms of dimension: 2D, 3D, and 2D with 3D information see Table 4. Two-dimensional solutions consider individual slices for detection while three-dimensional benefit from the spatial information, however, they suffer from higher computation cost. There is also an intermediate solution—using 2D images enriched with the information from adjacent slices.

In the majority of reported research, the CMB detection process is broken down into two stages: *CMB Candidates Detection*, and *CMB Candidates Verification* (see Table 4). This division is necessary due to the resemblances between CMBs and their mimics, which can result in a high number of false-positive candidates after *CMB Candidates Detection* stage. In order to reduce FP candidates, the *CMB Candidates verification* is necessary. Although it may increase computation time, it gives the opportunity to obtain more reliable results. Nevertheless, maintaining a balance between accuracy and efficiency is crucial, especially when considering real-time usage.

Another issue worth considering is the nature of cerebral microbleeds. Due to the fact that they are small hemorrhages, it can be challenging to detect them, even by an experienced radiologist. Therefore, the system designed to identify CMBs should be sensitive to such small objects. Automatic systems may prove to be more effective in this regard since they can analyze information that is not visible to the human eye. It is also proven that using more accurate and sensitive MRI machines with properly adjusted parameters can increase the likelihood of detecting all microbleeds, even very small ones. Nandigam et al. (2009).

Another problem relates to the possibility of overlooking some CMBs by an experienced rater. In any research regarding detection, establishing a ground truth is necessary. However, this can be extremely challenging since the level of rater agreement may be relatively low, such as $\kappa = 0.68$ (Seghier et al., 2011). To reduce this problem, the initial rating should involve as many raters as possible. Additionally, verification of system results may be useful, as some CMBs that were missed by raters may be detected by the system and should not be considered false-positive (Momeni et al., 2021). On the other hand, radiologists have the advantage of being able to view potential CMB from multiple perspectives and consult with teammates, which is not possible for an automated system Therefore, providing additional information such as gender, age, injury, angiography scans, etc. may also prove to be beneficial (Kuijf et al., 2013).

From a clinical application perspective, certain practical respects must also be taken into account when designing a CMB detection system. It is crucial to keep the end user's perspective in mind. Therefore, when presenting results, the format should be designed with the user experience in mind.

Providing a bounding-box or a circle as an indicator is crucial, but including further information such as the confidence score of the prediction can be highly beneficial. The machine-learning system typically generates this value, and it might offer the radiologist insight into the level of certainty, which can hasten the evaluation process. We also suggest to present the results using medical rating scales like MARS (Gregoire et al., 2009) BOMBS (Cordonnier et al., 2009) (see Section 2.2) for a more comprehensive interpretation.

Furthermore, it is essential to incorporate the ability to accept or reject a given prediction, by the end-user. As the system to be developed is a computer-aided system, the user must have the possibility to agree or disagree with the proposed outcome since their decision is final. A highly desirable feature of the system is also the automatic incorporation of such decisions through system retraining. However, it is crucial to distinguish this decision from involving a human in the loop. The raters possess indispensable knowledge for CMBs rating and may be utilized during system design, such as to validate preliminary results or to label extracted candidates as CMB and non-CMB, similar to Chen et al. (2019). Nevertheless, they should not be employed as the final stage of the process to enhance system performance. The reported 100% precision or specificity of a semi-automated system where a human is part of the FP reduction process is simply misleading (Barnes et al., 2011; Kuijf et al., 2013; Morrison et al., 2018). Even though such semi-automated system significantly reduces the time required for a single scan rating, this evaluation approach is confusing. Nonetheless, feedback from the radiologist regarding the prediction may be utilized for instance for continual learning (Pianykh et al., 2020). Such an approach could lead to improvements in an already working system.

Having analyzed existing approaches we concluded that ML-based computer-aided systems report significantly higher results than classical image analysis systems. Furthermore, over the years, they have become increasingly popular and widely adopted. ML-based systems can be divided into two main groups considering the main approach: classification and detection/segmentation. Some scholars report performing microbleed detection by dividing the image into small pieces and classifying them as either containing or not a microbleed. Whereas others perform direct detection or segmentation on the whole image.

In our opinion, the most promising approaches appear to be those that combine two-dimensional analysis with 3D information, incorporating neural network-based detection along with an additional cerebral microbleed verification process. Considering the nature of the cerebral microbleeds, two primary challenges arise in their detection: small sizes and similarity to other objects visible in the MRI. An appropriate selection of the neural network may effectively address the first challenge. Detecting small objects has been a challenge since the early stages of machine learning-based system development. According to Cheng et al. (2023), the state-of-the-art architectures for small object detection are RoI Transformer (Ding et al., 2019) and Oriented R-CNN (Xie et al., 2021). Therefore, we recommend focusing on these architectures for further research.

4.4. Evaluation

Section 3.4 highlighted another crucial aspect to consider—system evaluation, in which we presented various metrics and their correlations. Ensuring that the system works effectively, reliably, and achieves its intended purpose is vital. Therefore, it is necessary to select evaluation metrics that accurately determine the system's performance and whether it meets the required specifications. Additionally, the chosen evaluation metrics should align with the task's specific requirements to ensure optimal performance. The metrics used may differ depending on the selected task, such as classification, detection, or segmentation. In our opinion, it is crucial to report and analyze as many metrics as possible when evaluating the system because they focus on different aspects of the system's performance. While achieving a sensitivity of 99% may initially appear as an outstanding result, it is not satisfactory if it is confronted with a precision of only 40%. Researchers may emphasize the importance of sensitivity while downplaying the number of potential false positives, but this can be detrimental to the system's reliability and overall synthesis, like in Barnes et al. (2011). Therefore, it is crucial to design a system that is balanced and optimized as a whole to ensure optimal performance.

System evaluation plays a crucial role in enabling comparison between different approaches. As demonstrated in Table 4, it is apparent that the researchers do not always provide all the necessary metrics required for accurate comparisons. This lack of information can significantly impede the identification of the current state-of-the-art and hinder the comparison of different approaches. Therefore, it is essential to present all relevant metrics to ensure accurate comparison and the superiority of one approach over another can be determined.

Moreover, we suggest employing methods like k-fold validation during the system development that can aid better evaluation within the same dataset. The obtained results may differ depending on chosen training, validation, and testing sets, making k-fold validation a recommended approach (Al-masni et al., 2020a, 2020b; Ferlin et al., 2021).

Another important aspect that we would like to draw attention to is providing technical details regarding the system, for instance by preparation of a system nameplate. It could contain a comprehensive description of system properties and target data type. Moreover, there should be information about hardware and selected parameters to

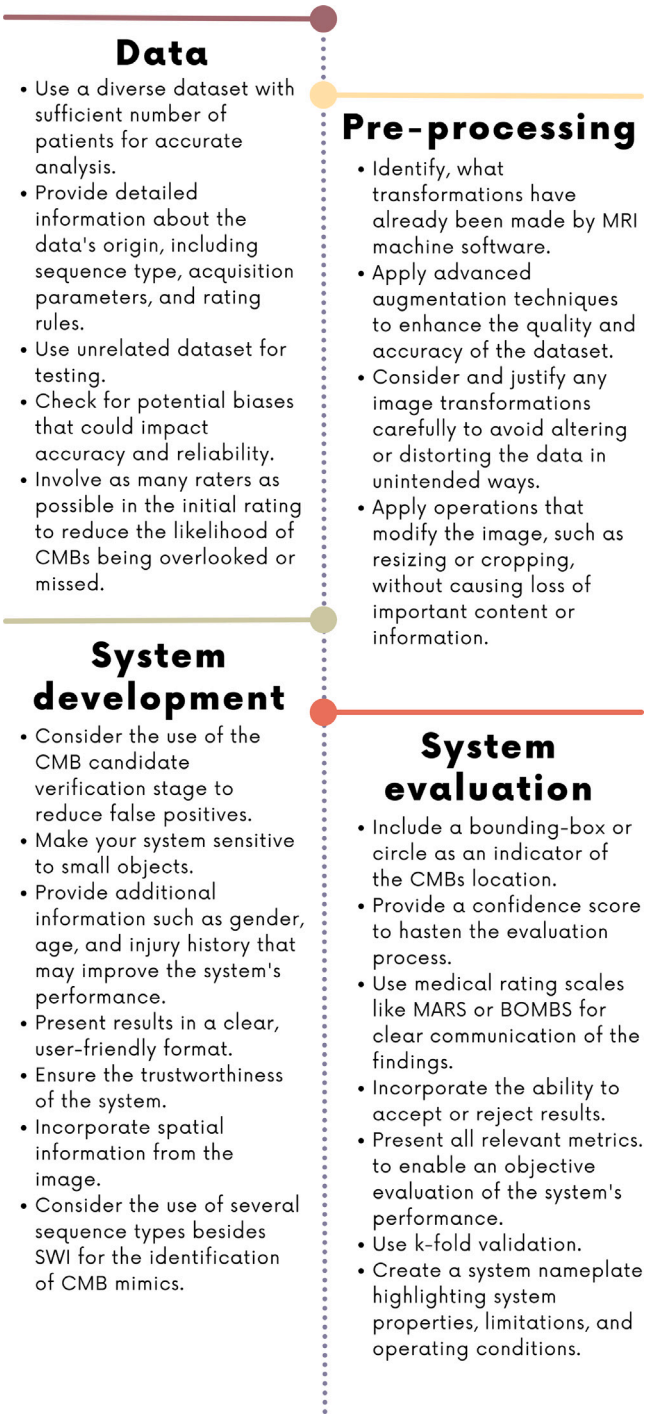

Fig. 8. Guidelines for the synthesis of an automatic CMB detection system.

make the system reproducible. It should also highlight the operating conditions of the system as well as its limitations.

In addition to the importance of providing relevant metrics for system evaluation and obtaining high scores on those metrics, we believe that there is a broader issue of system trustworthiness that needs to be considered. While traditional image transformations and morphological operations are relatively straightforward to explain, the interpretability of black-box machine-learning systems remains a significant challenge (Amann et al., 2020; Angelov et al., 2021; Barredo Arrieta et al., 2020). This issue is particularly important in medicine, where the decision-making process must be transparent to ensure that conclusions are based on the correct grounds rather than any inherent bias. It has been also raised by many researchers in the field of CMB detection (Chen et al., 2019; Chesebro et al., 2021; Ferlin et al., 2021; Hong, Cheng, Zhang, 2019; Lu et al., 2017; Morrison et al., 2018; Myung et al., 2021), but none of them has actually implemented it. Thus, reducing bias is crucial to ensure that AI systems used in medicine are reliable and trustworthy (Mikołajczyk et al., 2021). In this regard, guidelines for designing responsible and trustworthy AI systems have been proposed by experts in the field, such as those presented for example by GoogleAI (GoogleAI, 2018). These guidelines emphasize the importance of transparency, explainability, and interpretability in AI systems, which can aid in establishing trust and mitigating any concerns regarding potential biases. We would like to emphasize the importance of addressing the issue of system trustworthiness to foster the widespread adoption of AI systems in the medical field. It is crucial to ensure that these systems are utilized safely and effectively to benefit patients and healthcare providers.

5. Conclusions

One of the results of our research is a set of good practices and recommendations, which we have presented in Fig. 8. This guide is designed to assist researchers in their work and we are confident that it will be a useful tool for those working in this area of research. By following these guidelines, it is anticipated that more efficient automatic CMB detection systems can be developed.

To the best of our knowledge, this paper represents the first comprehensive collation of all available research regarding automatic CMB detection. By highlighting the limitations and challenges of current approaches and identifying areas where improvements can be made, we aimed to provide a valuable resource of knowledge and ideas for further research within this domain. Given the medical character of this task and the significant implications for patient care, it is essential to establish reliable and accurate methods for detecting CMBs. By providing a detailed analysis of existing research, we hope to inspire new avenues of investigation and encourage a more comprehensive and rigorous evaluation of obtained results. Concluding, this paper makes a significant contribution to the field of automatic cerebral microbleeds detection, and paving the way for further advancements in this area. We believe that our findings will be of great value to researchers, clinicians, and other stakeholders working in this area. We hope that this paper will serve as a catalyst for better practices in knowledge sharing and collaboration between different research groups, as well as, stimulate further research and lead to improved system outcomes.

CRediT authorship contribution statement

Maria Ferlin: Conceptualization, Methodology, Investigation, Resources, Data curation, Writing – original draft, Writing – review & editing, Visualization, Project administration. **Zuzanna Klawikowska:** Conceptualization, Methodology, Investigation, Resources, Data curation, Writing – original draft, Writing – review & editing, Visualization. **Michał Grochowski:** Conceptualization, Methodology, Formal analysis, Writing – original draft, Writing – review & editing, Supervision, Funding acquisition. **Małgorzata Grzywińska:** Validation, Writing – review & editing. **Edyta Szurowska:** Validation, Writing – review & editing, Supervision.

Declaration of competing interest

The authors declare that they have no known competing financial interests or personal relationships that could have appeared to influence the work reported in this paper.

Data availability

No data was used for the research described in the article.

Table A.5
Comparison of additional dataset acquisition parameters used in the reviewed approaches. Supplement information to Table 3.

Reference	TR [ms]	TE [ms]	FA [°]	BW [Hz/px]	Rating
Kuijf et al. (2011)	20	2.5/15	–	–	MARS
Barnes et al. (2011)	57	40	20	–	Ayaz et al. (2010)
Hong, Cheng, Wang (2019), Hong, Cheng, Zhang (2019), Hong et al. (2020)	–	20	15	120	MARS
Bian et al. (2013) and Morrison et al. (2018)	56	28	20	–	Similar to BOMBS/MARS
Kuijf et al. (2012)	20 T2 ∗ W, 7 T1W	2.5/15 T2 ∗ W, 3 T1W	–	–	MARS
Lu, Liu, Wang et al. (2021), Lu, Nayak et al. (2021), Zhang, Hou et al. (2018), Zhang et al. (2016), Zhang, Zhang et al. (2018), and Wang et al. (2017, 2019)	28	20	15	120	MARS
Afzal et al. (2022)	17	24	–	–	Micro-drain functional rating scale
Chen et al. (2015)	–	–	–	–	–
Liu et al. (2020)	17	24	–	–	MARS
Vieira (2023)	17	24	–	–	MARS
Ateeq et al. (2018)	17	24	–	–	MARS
Rashid et al. (2021)	1900 T1W MPRAGE (T1WMP), 3200 T2W, 35 SWI	2.93 T1WMP, 408 T2W, 7.5/ 15/ 22.5/ 30 SWI	9 T1WMP, 120 T2W, 15 SWI	170 T1WMP, 750 T2W, 200 SWI	Inspired by BOMBS
Sa-ngiem et al. (2019)	–	–	–	–	–
Roy et al. (2015)	–	25	–	–	–
Fazlollahi et al. (2013)	–	–	–	–	–
Fazlollahi et al. (2014)	27 SWI, 2.3 T1W	20 SWI, 2.98 T1W	20 SWI, 9 T1W	–	MARS
Dou et al. (2015)	–	–	–	–	MARS
van den Heuvel et al. (2015, 2016)	27 SWI, 2300 T1MPR	20 SWI, 2.98 T1MPR	15 SWI, 9 T1MPR	120 SWI, 240T1 MPR	MARS
Li et al. (2021)	5727 T2 FRFSE (T2F), 77.3 SWAN-W, 8400 T2W FLAIR (T2WF)	93 T2F, 45 SWAN-W, 145 T2WF	15 SWAN-W, 145 T2WF	833 T2F & T2WF, 625 SWAN-W	–
Fazlollahi et al. (2015)	27 SWI, 2.3 T1W	20 SWI, 2.98 T1W	20 SWI, 9 T1W	–	MARS
Chesebro et al. (2021)	6.6 T1W, 17 T2 ∗ W SWI, 15 T2 ∗ W GRE	3 T1W, 24 T2 ∗ W SWI, 22 T2 ∗ W GRE	–	–	Greenberg et al. (2009)
Kuijf et al. (2013)	1653 T2 ∗ W, 11000 FLAIR, 7.9 T1W	20 T2 ∗ W, 125 FLAIR, 4.5 T1W	–	–	MARS
Chen et al. (2019)	40 SWI, 50 3DSPGR	2.4/12/14.3/20.3 SWI, 16 3DSPGR	25	–	computer-aided detection developed by Bian et al. (2013) with rater
Seghier et al. (2011)	6000 T2W Fast Spin Echo (T2WFSE), 300 T2 ∗ GRE	105 T2WFSE, 40 T2 ∗ GRE	20 T2 ∗ GRE	–	MARS
Koschmieder et al. (2022)	2300 T1 MP-RAGE 27 SWI	2.98 T1 MP-RAGE 20 SWI	9 T1 MP-RAGE 15 SWI	240 T1 MP-RAGE 120 SWI	Greenberg et al. (2009)
Kim et al. (2022)	27	20	15	120	–
Lee et al. (2022)	27 DS1, 28 DS2	20	15	–	Greenberg et al. (2009)

(*continued on next page*)

Appendix. Supplementary details for data set

See Table A.5.

Table A.5 (*continued*).

Al-masni et al. (2020a, 2020b)	27 HR, 40 LR	20 HR, 13.7 LR	15	120	Greenberg et al. (2009)
Myung et al. (2021)	1050	20	21	–	–
Ferlin et al. (2021)	17 DS1, 27 DS2, 40 DS2	24 DS1, 20 DS2, 13.7 DS2	15 DS2	120 DS2	MARS DS1, Greenberg et al. (2009) DS2
Momeni et al. (2021)	27 SWI, 2.3 T1W	20 SWI, 2.98 T1W	20 SWI, 9 T1W	–	MARS
Liu et al. (2019)	49/50 1.5T, 27-34 3T	40 1.5T, 17.5-20 3T	15 1.5T, 12/15 3T	80 1.5T, 100-425 3T	–
Ferrer et al. (2023)	27 DS1, 17 DS2	20 DS1, 24 DS2	20 DS1	–	MARS DS1 & DS2, Lu, Liu, MacKinnon et al. (2021) DS3
Ghafaryasl et al. (2012)	–	–	–	–	–
Sundaresan et al. (2022)	504 T2*-GRE, 27 SWI	15 T ∗ 2-GRE, 9.4/20 SWI	–	–	MARS
Dou et al. (2016)	17	24	–	–	MARS
Stanley and Franklin (2022b)	17	24	–	–	MARS
Stanley and Franklin (2022a)	17 SWI, 27/40 SVS	24 SWI, 20/14 SVS	15 SVS	120 SVS	MARS SWI/Greenberg et al. (2009) SVS

References

Afzal, S., Khan, I., & Lee, J. (2022). A transfer learning-based approach to detect cerebral microbleeds. *Computers, Materials & Continua*, [ISSN: 1546-2218] *71*(1), 1903. http://dx.doi.org/10.32604/cmc.2022.021930.

Akiyama, Y., Miyata, K., Harada, K., Minamida, Y., Nonaka, T., Koyanagi, I., Asai, Y., & Houkin, K. (2009). Susceptibility-weighted magnetic resonance imaging for the detection of cerebral microhemorrhage in patients with traumatic brain injury. *Neurologia Medico-Chirurgica*, *49*(3), 97–99. http://dx.doi.org/10.2176/nmc.49.97, ISSN: 0470-8105, 1349-8029.

Akoudad, S., Portegies, M. L. P., Koudstaal, P. J., Hofman, A., van der Lugt, A., Ikram, M. A., & Vernooij, M. W. (2015). Cerebral microbleeds are associated with an increased risk of stroke: The rotterdam study. *Circulation*, [ISSN: 1524-4539] *132*(6), 509–516. http://dx.doi.org/10.1161/CIRCULATIONAHA.115.016261, (Electronic).

Al-masni, M. A., Kim, W. R., Kim, E. Y., Noh, Y., & Kim, D. H. (2020a). Automated detection of cerebral microbleeds in MR images: A two-stage deep learning approach. *NeuroImage: Clinical*, [ISSN: 2213-1582] *28*, Article 102464. http://dx.doi.org/10.1016/j.nicl.2020.102464.

Al-masni, M. A., Kim, W.-R., Kim, E. Y., Noh, Y., & Kim, D.-H. (2020b). A two cascaded network integrating regional-based YOLO and 3D-CNN for cerebral microbleeds detection. In *2020 42nd annual international conference of the IEEE engineering in medicine & biology society (EMBC)* (pp. 1055–1058). IEEE, ISBN: 978-1-72811-990-8, http://dx.doi.org/10.1109/EMBC44109.2020.9176073.

Amann, J., Blasimme, A., Vayena, E., Frey, D., Madai, V. I., & the Precise4Q consortium (2020). Explainability for artificial intelligence in healthcare: a multidisciplinary perspective. *BMC Medical Informatics and Decision Making*, [ISSN: 1472-6947] *20*(1), 310. http://dx.doi.org/10.1186/s12911-020-01332-6.

Angelov, P. P., Soares, E. A., Jiang, R., Arnold, N. I., & Atkinson, P. M. (2021). Explainable artificial intelligence: an analytical review. *WIREs Data Mining and Knowledge Discovery*, *11*(5), http://dx.doi.org/10.1002/widm.1424, ISSN: 1942-4787, 1942-4795.

Ashburner, J., Barnes, G., Chen, C.-C., Daunizeau, J., Flandin, G., Friston, K., Gitelman, D., Glauche, V., Henson, R., Hutton, C., Jafarian, A., Kiebel, S., Kilner, J., Litvak, V., Mattout, J., Moran, R., Penny, W., Phillips, C., Razi, A., & Zeidman, P. (2021). SPM12 manual. https://www.fil.ion.ucl.ac.uk/spm/software/spm12/.

Ashburner, J., & Friston, K. J. (2005). Unified segmentation. *NeuroImage*, [ISSN: 10538119] *26*(3), 839–851. http://dx.doi.org/10.1016/j.neuroimage.2005.02.018.

Ateeq, T., Majeed, M. N., Anwar, S. M., Maqsood, M., Rehman, Z.-u., Lee, J. W., Muhammad, K., Wang, S., Baik, S. W., & Mehmood, I. (2018). Ensemble-classifiers-assisted detection of cerebral microbleeds in brain MRI. *Computers & Electrical Engineering*, [ISSN: 00457906] *69*, 768–781. http://dx.doi.org/10.1016/j.compeleceng.2018.02.021.

Averbuch, A., & Shkolnisky, Y. (2003). 3D Fourier based discrete radon transform. *Applied and Computational Harmonic Analysis*, [ISSN: 1063-5203] *15*(1), 33–69. http://dx.doi.org/10.1016/S1063-5203(03)00030-7.

Ayaz, M., Boikov, A. S., Haacke, E. M., Kido, D. K., & Kirsch, W. M. (2010). Imaging cerebral microbleeds using susceptibility weighted imaging: one step toward detecting vascular dementia. *Journal of Magnetic Resonance Imaging: JMRI*, [ISSN: 1522-2586] *31*(1), 142–148. http://dx.doi.org/10.1002/jmri.22001.

Baid, U., Ghodasara, S., Mohan, S., Bilello, M., Calabrese, E., Colak, E., Farahani, K., Kalpathy-Cramer, J., Kitamura, F. C., Pati, S., Prevedello, L. M., Rudie, J. D., Sako, C., Shinohara, R. T., Bergquist, T., Chai, R., Eddy, J., Elliott, J., Reade, W., ... Bakas, S. (2021). The RSNA-ASNR-MICCAI brats 2021 benchmark on brain tumor segmentation and radiogenomic classification. ArXiv arXiv:2107.02314 [cs].

Bao, F., Shi, M., & Macdonald, F. (2018). Voxelwise detection of cerebral microbleed in CADASIL patients by naive Bayesian classifier. In *Proceedings of the 2018 international conference on information technology and management engineering (ICITME 2018)*. Atlantis Press, ISBN: 978-94-6252-607-5, http://dx.doi.org/10.2991/icitme-18.2018.35.

Barnard, E., & Casasent, D. (1989). A comparison between criterion functions for linear classifiers, with an application to neural nets. *IEEE Transactions on Systems, Man, and Cybernetics*, *19*(5), 1030–1041. http://dx.doi.org/10.1109/21.44018.

Barnes, S. R., Haacke, E. M., Ayaz, M., Boikov, A. S., Kirsch, W., & Kido, D. (2011). Semiautomated detection of cerebral microbleeds in magnetic resonance images. *Magnetic Resonance Imaging*, [ISSN: 0730725X] *29*(6), 844–852. http://dx.doi.org/10.1016/j.mri.2011.02.028.

Barredo Arrieta, A., Díaz-Rodríguez, N., Del Ser, J., Bennetot, A., Tabik, S., Barbado, A., Garcia, S., Gil-Lopez, S., Molina, D., Benjamins, R., Chatila, R., & Herrera, F. (2020). Explainable artificial intelligence (XAI): Concepts, taxonomies, opportunities and challenges toward responsible AI. *Information Fusion*, [ISSN: 1566-2535] *58*, 82–115. http://dx.doi.org/10.1016/j.inffus.2019.12.012.

Bian, W., Hess, C. P., Chang, S. M., Nelson, S. J., & Lupo, J. M. (2013). Computer-aided detection of radiation-induced cerebral microbleeds on susceptibility-weighted MR images. *NeuroImage: Clinical*, [ISSN: 22131582] *2*, 282–290. http://dx.doi.org/10.1016/j.nicl.2013.01.012.

Bian, W., Hess, C. P., Chang, S. M., Nelson, S. J., & Lupo, J. M. (2014). Susceptibility-weighted MR imaging of radiation therapy-induced cerebral microbleeds in patients with glioma: a comparison between 3T and 7T. *Neuroradiology*, *56*(2), 91–96. http://dx.doi.org/10.1007/s00234-013-1297-8, ISSN: 0028-3940, 1432-1920.

Bian, W., Morrison, M. A., Zhu, X., Avadiappan, S., Chen, Y., Payabvash, S., Shah, M., Hess, C. P., & Lupo, J. M. (2018). CMB labeler. https://github.com/LupoLab-UCSF/CMB_labeler.

Binczyk, F., Stjelties, B., Weber, C., Goetz, M., Meier-Hein, K., Meinzer, H.-P., Bobek-Billewicz, B., Tarnawski, R., & Polanska, J. (2017). Mimseg - an algorithm for automated detection of tumor tissue on NMR apparent diffusion coefficient maps. *Information Sciences*, [ISSN: 0020-0255] *384*, 235–248. http://dx.doi.org/10.1016/j.ins.2016.07.052.

Breiman, L. (2001). Random forests. *Machine Learning*, [ISSN: 1573-0565] *45*(1), 5–32. http://dx.doi.org/10.1023/A:1010933404324.

de Bresser, J., Brundel, M., Conijn, M., van Dillen, J., Geerlings, M., Viergever, M., Luijten, P., & Biessels, G. (2013). Visual cerebral microbleed detection on 7T MR imaging: Reliability and effects of image processing. *American Journal of Neuroradiology*, *34*(6), E61–E64. http://dx.doi.org/10.3174/ajnr.A2960, ISSN: 0195-6108, 1936-959X.

Buscema, M. (1998). Back propagation neural networks. *Substance Use & Misuse*, *33*(2), 233–270. http://dx.doi.org/10.3109/10826089809115863, ISSN: 1082-6084, 1532-2491.

Buslaev, A., Iglovikov, V. I., Khvedchenya, E., Parinov, A., Druzhinin, M., & Kalinin, A. A. (2020). Albumentations: Fast and flexible image augmentations. *Information*, [ISSN: 2078-2489] *11*(2), http://dx.doi.org/10.3390/info11020125.

Carass, A., Cuzzocreo, J., Wheeler, M. B., Bazin, P.-L., Resnick, S. M., & Prince, J. L. (2011). Simple paradigm for extra-cerebral tissue removal: Algorithm and analysis. *NeuroImage*, [ISSN: 10538119] *56*(4), 1982–1992. http://dx.doi.org/10.1016/j.neuroimage.2011.03.045.

Carass, A., Wheeler, M., Cuzzocreo, J., Bazin, P., Bassett, S., & Prince, J. (2007). A joint registration and segmentation approach to skull stripping. In *2007 4th IEEE international symposium on biomedical imaging: from nano to macro - proceedings*, *2007 4th IEEE international symposium on biomedical imaging* (pp. 656–659). ISBN: 1424406722, http://dx.doi.org/10.1109/ISBI.2007.356937.

Chang, C.-C., & Lin, C.-J. (2011). LIBSVM: A library for support vector machines. *ACM Transactions on Intelligent Systems and Technology*, *2*(3), 1–27. http://dx.doi.org/10.1145/1961189.1961199, ISSN: 2157-6904, 2157-6912.

Charidimou, A., Jäger, H. R., & Werring, D. J. (2012). Cerebral microbleed detection and mapping: Principles, methodological aspects and rationale in vascular dementia. *Experimental Gerontology*, [ISSN: 05315565] *47*(11), 843–852. http://dx.doi.org/10.1016/j.exger.2012.06.008.

Charidimou, A., Krishnan, A., Werring, D. J., & Rolf Jäger, H. (2013). Cerebral microbleeds: a guide to detection and clinical relevance in different disease settings. *Neuroradiology*, *55*(6), 655–674. http://dx.doi.org/10.1007/s00234-013-1175-4, ISSN: 0028-3940, 1432-1920.

Charidimou, A., Shams, S., Romero, J. R., Ding, J., Veltkamp, R., Horstmann, S., Eiriksdottir, G., van Buchem, M. A., Gudnason, V., Himali, J., Gurol, M. E., Viswanathan, A., Imaizumi, T., Vernooij, M. W., Seshadri, S., Greenberg, S. M., Benavente, O. R., Launer, L. J., & Shoamanesh, A. (2018). Clinical significance of cerebral microbleeds on MRI: A comprehensive meta-analysis of risk of intracerebral hemorrhage, ischemic stroke, mortality, and dementia in cohort studies (V1). *International Journal of Stroke : Official Journal of the International Stroke Society*, [ISSN: 1747-4930] *13*(5), 454–468. http://dx.doi.org/10.1177/1747493017751931.

Charidimou, A., & Werring, D. J. (2011). Cerebral microbleeds: detection, mechanisms and clinical challenges. *Future Neurology*, *6*(5), 587–611. http://dx.doi.org/10.2217/fnl.11.42, ISSN: 1479-6708, 1748-6971.

Chen, H., Dou, Q., Yu, L., Qin, J., Zhao, L., Mok, V. C. T., Wang, D., Shi, L., & Heng, P.-A. (2017). Chapter 6 - deep cascaded networks for sparsely distributed object detection from medical images. In S. K. Zhou, H. Greenspan, & D. Shen (Eds.), *Deep learning for medical image analysis* (pp. 133–154). Academic Press, ISBN: 978-0-12-810408-8, http://dx.doi.org/10.1016/B978-0-12-810408-8.00008-0.

Chen, Y., Villanueva-Meyer, J. E., Morrison, M. A., & Lupo, J. M. (2019). Toward automatic detection of radiation-induced cerebral microbleeds using a 3D deep residual network. *Journal of Digital Imaging*, [ISSN: 1618727X] *32*(5), 766–772. http://dx.doi.org/10.1007/s10278-018-0146-z.

Chen, H., Yu, L., Dou, Q., Shi, L., Mok, V. C. T., & Heng, P. A. (2015). Automatic detection of cerebral microbleeds via deep learning based 3D feature representation. In *2015 IEEE 12th international symposium on biomedical imaging (ISBI)* (pp. 764–767). IEEE, ISBN: 978-1-4799-2374-8, http://dx.doi.org/10.1109/ISBI.2015.7163984.

Cheng, A.-L., Batool, S., McCreary, C. R., Lauzon, M., Frayne, R., Goyal, M., & Smith, E. E. (2013). Susceptibility-weighted imaging is more reliable than T2*-weighted gradient-recalled echo MRI for detecting microbleeds. *Stroke*, *44*(10), 2782–2786. http://dx.doi.org/10.1161/STROKEAHA.113.002267, ISSN: 0039-2499, 1524-4628.

Cheng, G., Yuan, X., Yao, X., Yan, K., Zeng, Q., Xie, X., & Han, J. (2023). Towards large-scale small object detection: Survey and benchmarks. arXiv:2207.14096.

Chesebro, A. G., Amarante, E., Lao, P. J., Meier, I. B., Mayeux, R., & Brickman, A. M. (2021). Automated detection of cerebral microbleeds on T2*-weighted MRI. *Scientific Reports*, [ISSN: 20452322] *11*(1), 1–13. http://dx.doi.org/10.1038/s41598-021-83607-0.

Comon, P. (1995). Supervised classification: a probabilistic approach. In *ESANN95-european symposium on artificial neural networks* (pp. 111–128). University Press.

Conijn, M., Geerlings, M., Biessels, G.-J., Takahara, T., Witkamp, T., Zwanenburg, J., Luijten, P., & Hendrikse, J. (2011). Cerebral microbleeds on MR imaging: Comparison between 1.5 and 7T. *American Journal of Neuroradiology*, *32*(6), 1043–1049. http://dx.doi.org/10.3174/ajnr.A2450, ISSN: 0195-6108, 1936-959X.

Cordonnier, C., Al-Shahi Salman, R., & Wardlaw, J. (2007). Spontaneous brain microbleeds: systematic review, subgroup analyses and standards for study design and reporting. *Brain*, *130*(8), 1988–2003. http://dx.doi.org/10.1093/brain/awl387, ISSN: 0006-8950, 1460-2156.

Cordonnier, C., Potter, G. M., Jackson, C. A., Doubal, F., Keir, S., Sudlow, C. L., Wardlaw, J. M., & Al-Shahi Salman, R. (2009). Improving interrater agreement about brain microbleeds: Development of the brain observer MicroBleed scale (BOMBS). *Stroke*, [ISSN: 00392499] *40*(1), 94–99. http://dx.doi.org/10.1161/STROKEAHA.108.526996.

Cordonnier, C., & van der Flier, W. M. (2011). Brain microbleeds and Alzheimer's disease: innocent observation or key player? *Brain*, *134*(2), 335–344. http://dx.doi.org/10.1093/brain/awq321, ISSN: 1460-2156, 0006-8950.

Creswell, A., White, T., Dumoulin, V., Arulkumaran, K., Sengupta, B., & Bharath, A. A. (2018). Generative adversarial networks: An overview. *IEEE Signal Processing Magazine*, [ISSN: 1053-5888] *35*(1), 53–65. http://dx.doi.org/10.1109/MSP.2017.2765202.

Currie, S., Hoggard, N., Craven, I. J., Hadjivassiliou, M., & Wilkinson, I. D. (2013). Understanding MRI: basic MR physics for physicians. *Postgraduate Medical Journal*, *89*(1050), 209–223. http://dx.doi.org/10.1136/postgradmedj-2012-131342, ISSN: 0032-5473, 1469-0756.

Ding, J., Xue, N., Long, Y., Xia, G.-S., & Lu, Q. (2019). Learning RoI transformer for oriented object detection in aerial images. In *Proceedings of the IEEE/CVF conference on computer vision and pattern recognition*.

Doke, P., Shrivastava, D., Pan, C., Zhou, Q., & Zhang, Y.-D. (2020). Using CNN with Bayesian optimization to identify cerebral micro-bleeds. *Machine Vision and Applications*, *31*(5), 36. http://dx.doi.org/10.1007/s00138-020-01087-0, ISSN: 0932-8092, 1432-1769.

Dou, Q., Chen, H., Qin, J., & Heng, P.-A. (2020). CHAPTER NINE - automatic lesion detection with three-dimensional convolutional neural networks. In D. D. Feng (Ed.), *Biomedical engineering, Biomedical information technology (Second Edition)* (pp. 265–293). Academic Press, ISBN: 978-0-12-816034-3, http://dx.doi.org/10.1016/B978-0-12-816034-3.00009-2.

Dou, Q., Chen, H., Yu, L., Shi, L., Wang, D., Mok, V. C., & Heng, P. A. (2015). Automatic cerebral microbleeds detection from MR images via independent subspace analysis based hierarchical features. In *2015 37th annual international conference of the IEEE engineering in medicine and biology society (EMBC)* (pp. 7933–7936). IEEE, ISBN: 978-1-4244-9271-8, http://dx.doi.org/10.1109/EMBC.2015.7320232.

Dou, Q., Chen, H., Yu, L., Zhao, L., Qin, J., Wang, D., Mok, V. C., Shi, L., & Heng, P. A. (2016). Automatic detection of cerebral microbleeds from MR images via 3D convolutional neural networks. *IEEE Transactions on Medical Imaging*, [ISSN: 1558254X] *35*(5), 1182–1195. http://dx.doi.org/10.1109/TMI.2016.2528129.

Fan, P., Shan, W., Yang, H., Zheng, Y., Wu, Z., Chan, S. W., Wang, Q., Gao, P., Liu, Y., He, K., & Sui, B. (2022). Cerebral microbleed automatic detection system based on the "deep learning". *Frontiers in Medicine*, [ISSN: 2296-858X] *9*, Article 807443. http://dx.doi.org/10.3389/fmed.2022.807443.

Fazlollahi, A., Meriaudeau, F., Giancardo, L., Villemagne, V. L., Rowe, C. C., Yates, P., Salvado, O., & Bourgeat, P. (2015). Computer-aided detection of cerebral microbleeds in susceptibility-weighted imaging. *Computerized Medical Imaging and Graphics*, [ISSN: 08956111] *46*, 269–276. http://dx.doi.org/10.1016/j.compmedimag.2015.10.001.

Fazlollahi, A., Meriaudeau, F., Villemagne, V. L., Rowe, C. C., Desmond, P. M., Yates, P. A., Salvado, O., & Bourgeat, P. (2013). Automatic detection of small spherical lesions using multiscale approach in 3D medical images. In *2013 IEEE international conference on image processing* (pp. 1158–1162). IEEE, ISBN: 978-1-4799-2341-0, http://dx.doi.org/10.1109/ICIP.2013.6738239.

Fazlollahi, A., Meriaudeau, F., Villemagne, V. L., Rowe, C. C., Yates, P., Salvado, O., & Bourgeat, P. (2014). Efficient machine learning framework for computer-aided detection of cerebral microbleeds using the radon transform. In *2014 IEEE 11th international symposium on biomedical imaging (ISBI)* (pp. 113–116). IEEE, ISBN: 978-1-4673-1961-4, http://dx.doi.org/10.1109/ISBI.2014.6867822.

Ferlin, M. A., Grochowski, M., Kwasigroch, A., Mikołajczyk, A., Szurowska, E., Grzywińska, M., & Sabisz, A. (2021). A comprehensive analysis of deep neural-based cerebral microbleeds detection system. *Electronics*, [ISSN: 2079-9292] *10*(18), http://dx.doi.org/10.3390/electronics10182208.

Ferrer, N. R., Sagar, M. V., Klein, K. V., Kruuse, C., Nielsen, M., & Ghazi, M. M. (2023). Deep learning-based assessment of cerebral microbleeds in COVID-19. arxiv:2301.09322.

Filippi, M., Horsfield, M. A., Bressi, S., Martinelli, V., Baratti, C., Reganati, P., Campi, A., Miller, D. H., & Comi, G. (1995). Intra- and inter-observer agreement of brain MRI lesion volume measurements in multiple sclerosis: A comparison of techniques. *Brain*, [ISSN: 0006-8950] *118*(6), 1593–1600. http://dx.doi.org/10.1093/brain/118.6.1593.

Ghafaryasl, B., van der Lijn, F., Poels, M., Vrooman, H., Ikram, M. A., Niessen, W. J., van der Lugt, A., Vernooij, M., & de Bruijne, M. (2012). A computer aided detection system for cerebral microbleeds in brain MRI. In *2012 9th IEEE international symposium on biomedical imaging (ISBI)* (pp. 138–141). IEEE, http://dx.doi.org/10.1109/ISBI.2012.6235503.

GoogleAI (2018). Responsible AI practices. https://ai.google/responsibilities/responsible-ai-practices?category=general. Accessed: 2022-05-14.

Greenberg, S. M., Vernooij, M. W., Cordonnier, C., Viswanathan, A., Al-Shahi Salman, R., Warach, S., Launer, L. J., Van Buchem, M. A., & Breteler, M. M. (2009). Cerebral microbleeds: a guide to detection and interpretation. *The Lancet Neurology*, [ISSN: 14744422] *8*(2), 165–174. http://dx.doi.org/10.1016/S1474-4422(09)70013-4.

Gregoire, S. M., Chaudhary, U. J., Brown, M. M., Yousry, T. A., Kallis, C., Jäger, H. R., & Werring, D. J. (2009). The microbleed anatomical rating scale (MARS). *Neurology*, *73*(21), 1759. http://dx.doi.org/10.1212/WNL.0b013e3181c34a7d.

Gunter, J. L., Mead, A. K., Bermudez, C. L., Wiste, H. J., Gebre, R. K., Vemuri, P., Knopman, D. S., Petersen, R. C., Jack, C. R., Graff-Radford, J., & Cogswell, P. M. (2022). Improved automated cerebral microbleed (CMB) detection. *Alzheimer's & Dementia*, *18*, http://dx.doi.org/10.1002/alz.067992, ISSN: 1552-5260, 1552-5279.

Gunter, J. L., Spychalla, A. J., Ward, C. P., Graff-Radford, J., Huston, J., Kantarci, K., Knopman, D. S., Petersen, R. C., & Jack, C. R., Jr. (2018). P4-232: Automating cerebral microbleed detection in support of Alzheimer's disease trials using a convolutional neural network Ai. *Alzheimer's & Dementia*, [ISSN: 1552-5279] *14*(7), P1530–P1531. http://dx.doi.org/10.1016/j.jalz.2018.07.053.

Halabi, S. S., Prevedello, L. M., Kalpathy-Cramer, J., Mamonov, A. B., Bilbily, A., Cicero, M., Pan, I., Pereira, L. A., Sousa, R. T., Abdala, N., Kitamura, F. C., Thodberg, H. H., Chen, L., Shih, G., Andriole, K., Kohli, M. D., Erickson, B. J., & Flanders, A. E. (2019). The RSNA pediatric bone age machine learning challenge. *Radiology*, *290*(2), 498–503. http://dx.doi.org/10.1148/radiol.2018180736, ISSN: 0033-8419, 1527-1315.

Haller, S., Haacke, E. M., Thurnher, M. M., & Barkhof, F. (2021). Susceptibility-weighted imaging: Technical essentials and clinical neurologic applications. *Radiology*, *299*(1), 3–26. http://dx.doi.org/10.1148/radiol.2021203071, ISSN: 0033-8419, 1527-1315.

Haller, S., Vernooij, M. W., Kuijer, J. P. A., Larsson, E.-M., Jäger, H. R., & Barkhof, F. (2018). Cerebral microbleeds: imaging and clinical significance. *Radiology*, [ISSN: 0033-8419] *287*(1), 11–28. http://dx.doi.org/10.1148/radiol.2018170803.

He, K., Zhang, X., Ren, S., & Sun, J. (2016). Deep residual learning for image recognition. In *2016 IEEE conference on computer vision and pattern recognition* (pp. 770–778). http://dx.doi.org/10.1109/CVPR.2016.90.

Hodel, J., Rodallec, M., Gerber, S., Blanc, R., Maraval, A., Caron, S., Tyvaert, L., Zuber, M., & Zins, M. (2012). Séquences IRM SWAN, SWI et venobold exploitant le phénomène de susceptibilité magnétique : principes techniques et applications cliniques. *Journal of Neuroradiology*, [ISSN: 0150-9861] *39*(2), 71–86. http://dx.doi.org/10.1016/j.neurad.2011.11.006, language: French.

Hong, J., Cheng, H., Wang, S.-H., & Liu, J. (2019). Improvement of cerebral microbleeds detection based on discriminative feature learning. *Fundamenta Informaticae*, [ISSN: 1875-8681] *168*(2), 231–248. http://dx.doi.org/10.3233/FI-2019-1830.

Hong, J., Cheng, H., Zhang, Y. D., & Liu, J. (2019). Detecting cerebral microbleeds with transfer learning. *Machine Vision and Applications*, [ISSN: 14321769] *30*(7–8), 1123–1133. http://dx.doi.org/10.1007/s00138-019-01029-5.

Hong, J., Wang, S.-H., Cheng, H., & Liu, J. (2020). Classification of cerebral microbleeds based on fully-optimized convolutional neural network. *Multimedia Tools and Applications*, *79*(21–22), 15151–15169. http://dx.doi.org/10.1007/s11042-018-6862-z, ISSN: 1380-7501, 1573-7721.

Huang, G., Liu, Z., van der Maaten, L., & Weinberger, K. Q. (2018). Densely connected convolutional networks. arXiv:1608.06993.

Huang, G.-B., Zhu, Q.-Y., & Siew, C.-K. (2006). Extreme learning machine: Theory and applications. *Neurocomputing*, [ISSN: 09252312] *70*(1–3), 489–501. http://dx.doi.org/10.1016/j.neucom.2005.12.126.

Imaios (2009). Introduction to MRI sequences. ISBN: 978-1847537768, https://www.imaios.com/en/e-Courses/e-MRI/MRI-Sequences/MRI-sequences. Accessed: 2022-04-29.

Jain, A. K., & Ramaswami, M. D. (1988). Classifier design with parzen windows. In *Machine intelligence and pattern recognition*: *vol. 7*, *Pattern recognition and artificial intelligence* (pp. 211–228). North-Holland: http://dx.doi.org/10.1016/B978-0-444-87137-4.50021-7, ISSN: 0923-0459.

Jenkinson, M., Bannister, P., Brady, M., & Smith, S. (2002). Improved optimization for the robust and accurate linear registration and motion correction of brain images. *NeuroImage*, [ISSN: 10538119] *17*(2), 825–841. http://dx.doi.org/10.1006/nimg.2002.1132.

Jenkinson, M., Beckmann, C. F., Behrens, T. E., Woolrich, M. W., & Smith, S. M. (2012). FSL. *Neuroimage*, *62*(2), 782–790. http://dx.doi.org/10.1016/j.neuroimage.2011.09.015.

Jenkinson, M., & Smith, S. (2001). A global optimisation method for robust affine registration of brain images. *Medical Image Analysis*, [ISSN: 13618415] *5*(2), 143–156. http://dx.doi.org/10.1016/S1361-8415(01)00036-6.

Kaaouana, T., Bertrand, A., Ouamer, F., Law-ye, B., Pyatigorskaya, N., Bouyahia, A., Thiery, N., Dufouil, C., Delmaire, C., Dormont, D., de Rochefort, L., & Chupin, M. (2017). Improved cerebral microbleeds detection using their magnetic signature on T2*-phase-contrast: A comparison study in a clinical setting. *NeuroImage: Clinical*, [ISSN: 22131582] *15*, 274–283. http://dx.doi.org/10.1016/j.nicl.2016.08.005.

Kim, J.-H., Al-masni, M. A., Lee, H.-J., Choi, Y.-S., & Kim, D.-H. (2022). A single-stage detector of cerebral microbleeds using 3D feature fused region proposal network (FFRP-net). In *2022 IEEE 4th international conference on artificial intelligence circuits and systems (AICAS)* (pp. 1–4). IEEE, ISBN: 978-1-66540-996-4, http://dx.doi.org/10.1109/AICAS54282.2022.9869855.

Klein, S., Staring, M., Murphy, K., Viergever, M., & Pluim, J. (2010). Elastix: A toolbox for intensity-based medical image registration. *IEEE Transactions on Medical Imaging*, *29*(1), 196–205. http://dx.doi.org/10.1109/TMI.2009.2035616, ISSN: 0278-0062, 1558-254X.

Koschmieder, K., Paul, M., van den Heuvel, T., van der Eerden, A., van Ginneken, B., & Manniesing, R. (2022). Automated detection of cerebral microbleeds via segmentation in susceptibility-weighted images of patients with traumatic brain injury. *NeuroImage: Clinical*, [ISSN: 22131582] *35*, Article 103027. http://dx.doi.org/10.1016/j.nicl.2022.103027.

Krizhevsky, A., Sutskever, I., & Hinton, G. E. (2012). Imagenet classification with deep convolutional neural networks. In F. Pereira, C. Burges, L. Bottou, & K. Weinberger (Eds.), *Advances in neural information processing systems, Vol. 25*. Curran Associates, Inc..

Kuijf, H. J., Brundel, M., de Bresser, J., van Veluw, S. J., Heringa, S. M., Viergever, M. A., Biessels, G. J., & Vincken, K. L. (2013). Semi-automated detection of cerebral microbleeds on 3.0 T MR images. *PLoS ONE*, [ISSN: 1932-6203] *8*(6), Article e66610. http://dx.doi.org/10.1371/journal.pone.0066610.

Kuijf, H. J., de Bresser, J., Biessels, G. J., Viergever, M. A., & Vincken, K. L. (2011). Detecting cerebral microbleeds in 7.0 t MR images using the radial symmetry transform. In *2011 IEEE international symposium on biomedical imaging: from nano to macro* (pp. 758–761). IEEE, ISBN: 978-1-4244-4127-3, http://dx.doi.org/10.1109/ISBI.2011.5872516.

Kuijf, H. J., de Bresser, J., Geerlings, M. I., Conijn, M. M., Viergever, M. A., Biessels, G. J., & Vincken, K. L. (2012). Efficient detection of cerebral microbleeds on 7.0t MR images using the radial symmetry transform. *NeuroImage*, [ISSN: 10538119] *59*(3), 2266–2273. http://dx.doi.org/10.1016/j.neuroimage.2011.09.061.

Lee, H., Battle, A., Raina, R., & Ng, A. Y. (2006). Efficient sparse coding algorithms. *Advances in Neural Information Processing Systems 19*, 8.

Lee, H., Kim, J.-H., Lee, S., Jung, K.-J., Kim, W.-R., Noh, Y., Kim, E. Y., Kang, K. M., Sohn, C.-H., Lee, D. Y., Al-masni, M. A., & Kim, D.-H. (2022). Detection of cerebral microbleeds in MR images using a single-stage triplanar ensemble detection network (TPE-det). *Journal of Magnetic Resonance Imaging*, http://dx.doi.org/10.1002/jmri.28487.

Leming, M., Das, S., & Im, H. (2022). Construction of a confounder-free clinical MRI dataset in the mass general brigham system for classification of Alzheimer's disease. *Artificial Intelligence in Medicine*, [ISSN: 09333657] *129*, Article 102309. http://dx.doi.org/10.1016/j.artmed.2022.102309.

Li, N., Wang, W.-T., Sati, P., Pham, D. L., & Butman, J. A. (2014). Quantitative assessment of susceptibility-weighted imaging processing methods. *Journal of Magnetic Resonance Imaging : JMRI*, [ISSN: 1522-2586] *40*(6), 1463–1473. http://dx.doi.org/10.1002/jmri.24501.

Li, T., Zou, Y., Bai, P., Li, S., Wang, H., Chen, X., Meng, Z., Kang, Z., & Zhou, G. (2021). Detecting cerebral microbleeds via deep learning with features enhancement by reusing ground truth. *Computer Methods and Programs in Biomedicine*, [ISSN: 18727565] *204*, http://dx.doi.org/10.1016/j.cmpb.2021.106051.

Lipton, M. L. (2008). Image contrast: T1, T2, T2, and proton density. In *Totally accessible MRI: A user's guide to principles, technology, and applications* (pp. 38–46). Springer, ISBN: 978-0-387-48896-7, http://dx.doi.org/10.1007/978-0-387-48896-7_4.

Liu, W., Anguelov, D., Erhan, D., Szegedy, C., Reed, S., Fu, C.-Y., & Berg, A. C. (2016). SSD: Single shot MultiBox detector. In B. Leibe, J. Matas, N. Sebe, & M. Welling (Eds.), *Computer vision – ECCV 2016, Vol. 9905* (pp. 21–37). Cham: Springer International Publishing, http://dx.doi.org/10.1007/978-3-319-46448-0_2, ISBN: 978-3-319-46447-3 978-3-319-46448-0.

Liu, S., Buch, S., Chen, Y., Choi, H.-S., Dai, Y., Habib, C., Hu, J., Jung, J.-Y., Luo, Y., Utriainen, D., Wang, M., Wu, D., Xia, S., & Haacke, E. M. (2017). Susceptibility weighted imaging: Current status and future directions. *NMR in Biomedicine*, [ISSN: 0952-3480] *30*(4), http://dx.doi.org/10.1002/nbm.3552.

Liu, J., Liu, T., de Rochefort, L., Ledoux, J., Khalidov, I., Chen, W., Tsiouris, A. J., Wisnieff, C., Spincemaille, P., Prince, M. R., & Wang, Y. (2012). Morphology enabled dipole inversion for quantitative susceptibility mapping using structural consistency between the magnitude image and the susceptibility map. *NeuroImage*, [ISSN: 10538119] *59*(3), 2560–2568. http://dx.doi.org/10.1016/j.neuroimage.2011.08.082.

Liu, H., Rashid, T., & Habes, M. (2020). Cerebral microbleed detection via Fourier descriptor with dual domain distribution modeling. In *2020 IEEE 17th international symposium on biomedical imaging workshops (ISBI workshops)* (pp. 1–4). http://dx.doi.org/10.1109/ISBIWorkshops50223.2020.9153365.

Liu, T., Surapaneni, K., Lou, M., Cheng, L., Spincemaille, P., & Wang, Y. (2012). Cerebral microbleeds: Burden assessment by using quantitative susceptibility mapping. *Radiology*, *262*(1), 269–278. http://dx.doi.org/10.1148/radiol.11110251, ISSN: 0033-8419, 1527-1315.

Liu, S., Utriainen, D., Chai, C., Chen, Y., Wang, L., Sethi, S. K., Xia, S., & Haacke, E. M. (2019). Cerebral microbleed detection using susceptibility weighted imaging and deep learning. *NeuroImage*, [ISSN: 10959572] *198*, 271–282. http://dx.doi.org/10.1016/j.neuroimage.2019.05.046.

Loy, G., & Zelinsky, A. (2003). Fast radial symmetry for detecting points of interest. *IEEE Transactions on Pattern Analysis and Machine Intelligence*, [ISSN: 0162-8828] *25*(8), 959–973. http://dx.doi.org/10.1109/TPAMI.2003.1217601.

Lu, D., Liu, J., MacKinnon, A. D., Tozer, D. J., & Markus, H. S. (2021). Prevalence and risk factors of cerebral microbleeds. *Neurology*, [ISSN: 0028-3878] *97*(15), e1493–e1502. http://dx.doi.org/10.1212/WNL.0000000000012673.

Lu, S., Liu, S., Wang, S.-H., & Zhang, Y.-D. (2021). Cerebral microbleed detection via convolutional neural network and extreme learning machine. *Frontiers in Computational Neuroscience*, [ISSN: 1662-5188] *15*, Article 738885. http://dx.doi.org/10.3389/fncom.2021.738885.

Lu, S., Lu, Z., Hou, X., Cheng, H., & Wang, S. (2017). Detection of cerebral microbleeding based on deep convolutional neural network. In *2016 13th international computer conference on wavelet active media technology and information processing, ICCWAMTIP 2017, Vol. 2018-Febru* (pp. 93–96). ISBN: 9781509061259, http://dx.doi.org/10.1109/ICCWAMTIP.2017.8301456.

Lu, S.-Y., Nayak, D. R., Wang, S.-H., & Zhang, Y.-D. (2021). A cerebral microbleed diagnosis method via FeatureNet and ensembled randomized neural networks. *Applied Soft Computing*, [ISSN: 1568-4946] *109*, Article 107567. http://dx.doi.org/10.1016/j.asoc.2021.107567.

Lu, S., Xia, K., & Wang, S.-H. (2020). Diagnosis of cerebral microbleed via VGG and extreme learning machine trained by Gaussian map bat algorithm. *Journal of Ambient Intelligence and Humanized Computing*, http://dx.doi.org/10.1007/s12652-020-01789-3, ISSN: 1868-5137, 1868-5145.

Lu, Z., Yan, Y., & Wang, S.-H. (2021). CMB-net: a deep convolutional neural network for diagnosis of cerebral microbleeds. *Multimedia Tools and Applications*, *81*(14), 19195–19214. http://dx.doi.org/10.1007/s11042-021-10566-z, ISSN: 1380-7501, 1573-7721.

Luo, L., Ye, L., Luo, M., Huang, D., Peng, H., & Yang, F. (2011). Methods of forward feature selection based on the aggregation of classifiers generated by single attribute. *Computers in Biology and Medicine*, [ISSN: 00104825] *41*(7), 435–441. http://dx.doi.org/10.1016/j.compbiomed.2011.04.005.

Lupo, J. M., Banerjee, S., Hammond, K. E., Kelley, D. A., Xu, D., Chang, S. M., Vigneron, D. B., Majumdar, S., & Nelson, S. J. (2009). GRAPPA-based susceptibility-weighted imaging of normal volunteers and patients with brain tumor at 7 T. *Magnetic Resonance Imaging*, [ISSN: 0730-725X] *27*(4), 480–488. http://dx.doi.org/10.1016/j.mri.2008.08.003.

Martinez-Ramirez, S., Greenberg, S. M., & Viswanathan, A. (2014). Cerebral microbleeds: overview and implications in cognitive impairment. *Alzheimer's Research & Therapy*, [ISSN: 1758-9193] *6*(3), 33. http://dx.doi.org/10.1186/alzrt263.

Mazurek, M., Papuć, E., & Rejdak, K. (2018). Czynniki wpływające na występowanie mikrokrwawień mózgowych. *Polski Przegląd Neurologiczny*, [ISSN: 1734-9745] *14*(3), 151–155, in polish.

Mikolajczyk, A., & Grochowski, M. (2018). Data augmentation for improving deep learning in image classification problem. In *2018 international interdisciplinary PhD workshop (IIPhDW)* (pp. 117–122). IEEE, ISBN: 978-1-5386-6143-7, http://dx.doi.org/10.1109/IIPHDW.2018.8388338.

Mikołajczyk, A., Grochowski, M., & Kwasigroch, A. (2021). Towards explainable classifiers using the counterfactual approach - global explanations for discovering bias in data. *Journal of Artificial Intelligence and Soft Computing Research*, [ISSN: 2083-2567] *11*(1), 51–67. http://dx.doi.org/10.2478/jaiscr-2021-0004.

Momeni, S., Fazlollahi, A., Yates, P., Rowe, C., Gao, Y., Liew, A. W.-C., & Salvado, O. (2021). Synthetic microbleeds generation for classifier training without ground truth. *Computer Methods and Programs in Biomedicine*, [ISSN: 0169-2607] *207*, Article 106127. http://dx.doi.org/10.1016/j.cmpb.2021.106127.

Morrison, M. A., Payabvash, S., Chen, Y., Avadiappan, S., Shah, M., Zou, X., Hess, C. P., & Lupo, J. M. (2018). A user-guided tool for semi-automated cerebral microbleed detection and volume segmentation_Evaluating vascular injury and data labelling for machine learning. *Neuroimage: Clinical*, 8. http://dx.doi.org/10.1016/j.nicl.2018.08.002.

Myung, M. J., Lee, K. M., Kim, H.-g., Oh, J., Lee, J. Y., Shin, I., Kim, E. J., & Lee, J. S. (2021). Novel approaches to detection of cerebral microbleeds: Single deep learning model to achieve a balanced performance. *Journal of Stroke and Cerebrovascular Diseases*, [ISSN: 1052-3057] *30*(9), Article 105886. http://dx.doi.org/10.1016/j.jstrokecerebrovasdis.2021.105886.

Nandigam, K., & Scully, M. A. (2013). SWAN MRI revealing multiple microhemorrhages secondary to septic emboli from mucormycosisauthor response. *Neurology*, *81*(2), 199–200. http://dx.doi.org/10.1212/01.wnl.0000432237.13307.12, ISSN: 0028-3878, 1526-632X.

Nandigam, R. N., Viswanathan, A., Delgado, P., Skehan, M. E., Smith, E. E., Rosand, J., Greenberg, S. M., & Dickerson, B. C. (2009). MR imaging detection of cerebral microbleeds: Effect of susceptibility-weighted imaging, section thickness, and field strength. *American Journal of Neuroradiology*, [ISSN: 01956108] *30*(2), 338–343. http://dx.doi.org/10.3174/ajnr.A1355.

Nikseresht, G., Agam, G., & Arfanakis, K. (2022). End-to-end task-guided refinement of synthetic images for data efficient cerebral microbleed detection. In *2022 26th international conference on pattern recognition (ICPR)* (pp. 2756–2763). IEEE, ISBN: 978-1-66549-062-7, http://dx.doi.org/10.1109/ICPR56361.2022.9956383.

Nusrat, I., & Jang, S.-B. (2018). A comparison of regularization techniques in deep neural networks. *Symmetry*, [ISSN: 2073-8994] *10*(11), 648. http://dx.doi.org/10.3390/sym10110648.

O'Shea, K., & Nash, R. (2015). An introduction to convolutional neural networks. Number: arXiv:1511.08458 [cs].

Park, J.-H., Park, S.-W., Kang, S.-H., Nam, T.-K., Min, B.-K., & Hwang, S.-N. (2009). Detection of traumatic cerebral microbleeds by susceptibility-weighted image of MRI. *Journal of Korean Neurosurgical Society*, [ISSN: 2005-3711] *46*(4), 365. http://dx.doi.org/10.3340/jkns.2009.46.4.365.

Paszke, A., Gross, S., Massa, F., Lerer, A., Bradbury, J., Chanan, G., Killeen, T., Lin, Z., Gimelshein, N., Antiga, L., Desmaison, A., Kopf, A., Yang, E., DeVito, Z., Raison, M., Tejani, A., Chilamkurthy, S., Steiner, B., Fang, L., ... Chintala, S. (2019). Pytorch: An imperative style, high-performance deep learning library. In *Advances in neural information processing systems 32* (pp. 8024–8035). Curran Associates, Inc..

Patterson, D. (2019). Neuroimaging core documentation. https://neuroimaging-core-docs.readthedocs.io/en/latest/index.html. Accessed: 2022-04-04.

Penny, W., Friston, K., Ashburner, J., Kiebel, S., & Nicholas, T. (2006). *Statistical parametric mapping: The analysis of functional* (1st ed.). Academic Press, ISBN: 978-0-12-372560-8.

Pianykh, O. S., Langs, G., Dewey, M., Enzmann, D. R., Herold, C. J., Schoenberg, S. O., & Brink, J. A. (2020). Continuous learning AI in radiology: Implementation principles and early applications. *Radiology*, *297*(1), 6–14. http://dx.doi.org/10.1148/radiol.2020200038, ISSN: 0033-8419, 1527-1315.

Poels, M. M., Ikram, M. A., van der Lugt, A., Hofman, A., Krestin, G. P., Breteler, M. M., & Vernooij, M. W. (2011). Incidence of cerebral microbleeds in the general population. *Stroke*, *42*(3), 656–661. http://dx.doi.org/10.1161/STROKEAHA.110.607184.

Poels, M., Ikram, M., van der Lugt, A., Hofman, A., Niessen, W., Krestin, G., Breteler, M., & Vernooij, M. (2012). Cerebral microbleeds are associated with worse cognitive function. *Neurology*, *78*(5), 326. http://dx.doi.org/10.1212/WNL.0b013e3182452928.

Preston, D. C. (2016). Magnetic resonance imaging (MRI) of the brain and spine: Basics. https://case.edu/med/neurology/NR/MRI%.htm. Accessed: 2023-05-17.

Rashid, T., Abdulkadir, A., Nasrallah, I. M., Ware, J. B., Liu, H., Spincemaille, P., Romero, J. R., Bryan, R. N., Heckbert, S. R., & Habes, M. (2021). DEEPMIR: a deep neural network for differential detection of cerebral microbleeds and iron deposits in MRI. *Scientific Reports*, [ISSN: 2045-2322] *11*(1), 14124. http://dx.doi.org/10.1038/s41598-021-93427-x.

Real, R., & Vargas, J. M. (1996). The probabilistic basis of Jaccard's index of similarity. *Systematic Biology*, *45*, 6.

Redmon, J., & Farhadi, A. (2017). YOLO9000: Better, faster, stronger. In *Proceedings of the IEEE conference on computer vision and pattern recognition*.

Ren, S., He, K., Girshick, R., & Sun, J. (2015). Faster R-CNN: Towards real-time object detection with region proposal networks. In *Proceedings of the 28th international conference on neural information processing systems - Volume 1* (pp. 91–99). MIT Press.

Revol-Muller, C., Peyrin, F., Carrillon, Y., & Odet, C. (2002). Automated 3D region growing algorithm based on an assessment function. *Pattern Recognition Letters*, [ISSN: 01678655] *23*(1–3), 137–150. http://dx.doi.org/10.1016/S0167-8655(01)00116-7.

Ronneberger, O., Fischer, P., & Brox, T. (2015). U-net: Convolutional networks for biomedical image segmentation. arXiv, arXiv:1505.04597.

Roy, S., Jog, A., Magrath, E., Butman, J. A., & Pham, D. L. (2015). Cerebral microbleed segmentation from susceptibility weighted images. In S. Ourselin, & M. A. Styner (Eds.), *Medical imaging 2015: image processing, Vol. 9413* (pp. 364–370). SPIE, http://dx.doi.org/10.1117/12.2082237.

Sa-ngiem, S., Dittakan, K., Temkiatvises, K., Yaisoongnern, S., & Kespechara, K. (2019). Cerebral microbleed detection by extracting area and number from susceptibility weighted imagery using convolutional neural network. *Journal of Physics: Conference Series*, *1229*(1), Article 012038. http://dx.doi.org/10.1088/1742-6596/1229/1/012038, ISSN: 1742-6588, 1742-6596.

Scheid, R., Ott, D. V., Roth, H., Schroeter, M. L., & von Cramon, D. Y. (2007). Comparative magnetic resonance imaging at 1.5 and 3 tesla for the evaluation of traumatic microbleeds. *Journal of Neurotrauma*, [ISSN: 0897-7151] *24*(12), 1811–1816. http://dx.doi.org/10.1089/neu.2007.0382.

Seghier, M. L., Kolanko, M. A., Leff, A. P., Jäger, H. R., Gregoire, S. M., & Werring, D. J. (2011). Microbleed detection using automated segmentation (MIDAS): A new method applicable to standard clinical MR images. *PLoS ONE*, [ISSN: 1932-6203] *6*(3), Article e17547. http://dx.doi.org/10.1371/journal.pone.0017547.

Seghier, M. L., Ramlackhansingh, A., Crinion, J., Leff, A. P., & Price, C. J. (2008). Lesion identification using unified segmentation-normalisation models and fuzzy clustering. *NeuroImage*, [ISSN: 10538119] *41*(4), 1253–1266. http://dx.doi.org/10.1016/j.neuroimage.2008.03.028.

Shams, S., Granberg, T., Martola, J., Li, X., Shams, M., Fereshtehnejad, S.-M., Cavallin, L., Aspelin, P., Kristoffersen-Wiberg, M., & Wahlund, L.-O. (2016). Cerebrospinal fluid profiles with increasing number of cerebral microbleeds in a continuum of cognitive impairment. *Journal of Cerebral Blood Flow and Metabolism : Official Journal of the International Society of Cerebral Blood Flow and Metabolism*, [ISSN: 1559-7016] *36*(3), 621–628. http://dx.doi.org/10.1177/0271678X15606141, (Electronic).

Shams, S., Martola, J., Cavallin, L., Granberg, T., Shams, M., Aspelin, P., Wahlund, L., & Kristoffersen-Wiberg, M. (2015). SWI or T2*: Which MRI sequence to use in the detection of cerebral microbleeds? The Karolinska imaging dementia study. *American Journal of Neuroradiology*, *36*(6), 1089–1095. http://dx.doi.org/10.3174/ajnr.A4248, ISSN: 0195-6108, 1936-959X.

Shattuck, D. W., & Leahy, R. M. (2002). BrainSuite: An automated cortical surface identification tool. *Medical Image Analysis*, 14.

Shoamanesh, A., Kwok, C., & Benavente, O. (2011). Cerebral microbleeds: Histopathological correlation of neuroimaging. *Cerebrovascular Diseases*, *32*(6), 528–534. http://dx.doi.org/10.1159/000331466, ISSN: 1421-9786, 1015-9770.

Siegel, E. L. (2019). What can we learn from the RSNA pediatric bone age machine learning challenge? *Radiology*, *290*(2), 504–505. http://dx.doi.org/10.1148/radiol.2018182657, ISSN: 0033-8419, 1527-1315.

Simonyan, K., & Zisserman, A. (2015). Very deep convolutional networks for large-scale image recognition. arXiv:1409.1556.

Singh, S. P., Wang, L., Gupta, S., Goli, H., Padmanabhan, P., & Gulyás, B. (2020). 3D deep learning on medical images: A review. *Sensors*, [ISSN: 1424-8220] *20*(18), 5097. http://dx.doi.org/10.3390/s20185097.

Sled, J., Zijdenbos, A., & Evans, A. (1998). A nonparametric method for automatic correction of intensity nonuniformity in MRI data. *IEEE Transactions on Medical Imaging*, [ISSN: 02780062] *17*(1), 87–97. http://dx.doi.org/10.1109/42.668698.

Smith, S. M. (2002). Fast robust automated brain extraction. *Human Brain Mapping*, *17*(3), 143–155. http://dx.doi.org/10.1002/hbm.10062, ISSN: 1065-9471, 1097-0193.

Soille, P. (2004). *Morphological image analysis*. Springer Berlin Heidelberg, http://dx.doi.org/10.1007/978-3-662-05088-0, ISBN: 978-3-642-07696-1 978-3-662-05088-0.

Song, S., Zheng, Y., & He, Y. (2017). A review of methods for bias correction in medical images. *Biomedical Engineering Review*, *3*(1), http://dx.doi.org/10.18103/bme.v3i1.1550, ISSN: 23759143, 23759151.

Standvoss, K., Crijns, T., Goerke, L., Janssen, D., Kern, S., van Niedek, T., van Vugt, J., Burgos, N. A., Gerritse, E. J., Mol, J., van de Vooren, D., Ghafoorian, M., van den Heuvel, T. L. A., & Manniesing, R. (2018). Cerebral microbleed detection in traumatic brain injury patients using 3D convolutional neural networks. In N. Petrick, & K. Mori (Eds.), *Medical imaging 2018: computer-aided diagnosis, Vol. 10575* (pp. 314–321). International Society for Optics and Photonics SPIE, http://dx.doi.org/10.1117/12.2294016.

Stanley, B. F., & Franklin, S. W. (2022a). Automated cerebral microbleed detection using selective 3D gradient co-occurance matrix and convolutional neural network. *Biomedical Signal Processing and Control*, [ISSN: 1746-8094] *75*, Article 103560. http://dx.doi.org/10.1016/j.bspc.2022.103560.

Stanley, B. F., & Franklin, S. W. (2022b). Effective feature extraction for cerebral microbleed detection using edge emphasized Weber maximum directional co-occurance matrix. *Journal of Ambient Intelligence and Humanized Computing*, http://dx.doi.org/10.1007/s12652-022-04023-4, ISSN: 1868-5137, 1868-5145.

Sundaresan, V., Arthofer, C., Zamboni, G., Dineen, R. A., Rothwell, P. M., Sotiropoulos, S. N., Auer, D. P., Tozer, D. J., Markus, H. S., Miller, K. L., Dragonu, I., Sprigg, N., Alfaro-Almagro, F., Jenkinson, M., & Griffanti, L. (2022). Automated detection of candidate subjects with cerebral microbleeds using machine learning. *Frontiers in Neuroinformatics*, [ISSN: 1662-5196] *15*, Article 777828. http://dx.doi.org/10.3389/fninf.2021.777828.

Suwalska, A., Wang, Y., Yuan, Z., Jiang, Y., Zhu, D., Chen, J., Cui, M., Chen, X., Suo, C., & Polanska, J. (2022). CMB-HUNT: Automatic detection of cerebral microbleeds using a deep neural network. *Computers in Biology and Medicine*, [ISSN: 00104825] *151*, Article 106233. http://dx.doi.org/10.1016/j.compbiomed.2022.106233.

Tajudin, A. S., Sulaiman, S. N., Isa, I. S., Soh, Z. H. C., Karim, N. K. A., & Shuaib, I. L. (2017). Microbleeds detection using watershed-driven active contour. In *2017 7th IEEE international conference on control system, computing and engineering (ICCSCE)* (pp. 320–324). IEEE, ISBN: 978-1-5386-3897-2, http://dx.doi.org/10.1109/ICCSCE.2017.8284427.

Tao, Y., & Cloutie, R. S. (2018). Voxelwise detection of cerebral microbleed in CADASIL patients by genetic algorithm and back propagation neural network. In *Proceedings of the 2018 3rd international conference on communications, information management and network security (CIMNS 2018)*. Atlantis Press, ISBN: 978-94-6252-620-4, http://dx.doi.org/10.2991/cimns-18.2018.23.

Tharwat, A. (2016). Linear vs. quadratic discriminant analysis classifier: a tutorial. *International Journal of Applied Pattern Recognition*, *3*(2), 145. http://dx.doi.org/10.1504/IJAPR.2016.079050, ISSN: 2049-887X, 2049-8888.

Tsushima, Y., Tanizaki, Y., Aoki, J., & Endo, K. (2002). MR detection of microhemorrhages in neurologically healthy adults. *Neuroradiology*, *44*(1), 31–36. http://dx.doi.org/10.1007/s002340100649, ISSN: 0028-3940, 1432-1920.

Tustison, N. J., Avants, B. B., Cook, P. A., Zheng, Y., Egan, A., Yushkevich, P. A., & Gee, J. C. (2010). N4ITK: Improved N3 bias correction. *IEEE Transactions on Medical Imaging*, *29*(6), 1310–1320. http://dx.doi.org/10.1109/TMI.2010.2046908, ISSN: 0278-0062, 1558-254X.

van den Heuvel, T. L. A., Ghafoorian, M., van der Eerden, M. D. A. W., Goraj, B. M., Andriessen, T. M. J. C., ter Haar Romeny, B. M., & Platel, B. (2015). Computer aided detection of brain micro-bleeds in traumatic brain injury. In *Society of photo-optical instrumentation engineers (SPIE) conference series*: *vol. 9414*, *Medical imaging 2015: computer-aided diagnosis* (p. 94142F). http://dx.doi.org/10.1117/12.2075353.

van den Heuvel, T., van der Eerden, A., Manniesing, R., Ghafoorian, M., Tan, T., Andriessen, T., Vande Vyvere, T., van den Hauwe, L., ter Haar Romeny, B., Goraj, B., & Platel, B. (2016). Automated detection of cerebral microbleeds in patients with traumatic brain injury. *NeuroImage: Clinical*, [ISSN: 22131582] *12*, 241–251. http://dx.doi.org/10.1016/j.nicl.2016.07.002.

Vernooij, M. W., Ikram, M. A., Wielopolski, P. A., Krestin, G. P., Breteler, M. M. B., & van der Lugt, A. (2008). Cerebral microbleeds: Accelerated 3D T2*-weighted GRE MR imaging versus conventional 2D T2*-weighted GRE MR imaging for detection. *Radiology*, [ISSN: 0033-8419] *248*(1), 272–277. http://dx.doi.org/10.1148/radiol.2481071158.

Vieira, A. A. (2023). *Integrating the spatial pyramid pooling into 3D convolutional neural networks for cerebral microbleeds detection* (Ph.D. thesis), College of Computing and Engineering Nova Southeastern University.

Wang, S.-C. (2003). Artificial neural network. In *Interdisciplinary computing in java programming* (pp. 81–100). Springer US, ISBN: 978-1-4615-0377-4, http://dx.doi.org/10.1007/978-1-4615-0377-4_5.

Wang, S., Jiang, Y., Hou, X., Cheng, H., & Du, S. (2017). Cerebral micro-bleed detection based on the convolution neural network with rank based average pooling. *IEEE Access*, [ISSN: 2169-3536] *5*, 16576–16583. http://dx.doi.org/10.1109/ACCESS.2017.2736558.

Wang, S., Sun, J., Mehmood, I., Pan, C., Chen, Y., & Zhang, Y.-D. (2020). Cerebral micro-bleeding identification based on a nine-layer convolutional neural network with stochastic pooling. *Concurrency Computations: Practice and Experience*, *32*(1), http://dx.doi.org/10.1002/cpe.5130, ISSN: 1532-0626, 1532-0634.

Wang, S., Tang, C., Sun, J., & Zhang, Y. (2019). Cerebral micro-bleeding detection based on densely connected neural network. *Frontiers in Neuroscience*, [ISSN: 1662453X] *13*, 1–11. http://dx.doi.org/10.3389/fnins.2019.00422.

Werring, D. J. (2004). Cognitive dysfunction in patients with cerebral microbleeds on T2*-weighted gradient-echo MRI. *Brain*, [ISSN: 1460-2156] *127*(10), 2265–2275. http://dx.doi.org/10.1093/brain/awh253.

Werring, D. J. (2007). Cerebral microbleeds: Clinical and pathophysiological significance. *Journal of Neuroimaging*, *17*(3), 193–203. http://dx.doi.org/10.1111/j.1552-6569.2006.00070.x, ISSN: 10512284, 15526569.

World Health Organization (2020). Global health estimates 2020: Deaths by cause, age, sex, by country and by region, 2000–2019.

Xie, X., Cheng, G., Wang, J., Yao, X., & Han, J. (2021). Oriented R-CNN for object detection. In *Proceedings of the IEEE/CVF international conference on computer vision* (pp. 3520–3529).

Yakushiji, Y., Nishiyama, M., Yakushiji, S., Hirotsu, T., Uchino, A., Nakajima, J., Eriguchi, M., Nanri, Y., Hara, M., Horikawa, E., & Kuroda, Y. (2008). Brain microbleeds and global cognitive function in adults without neurological disorder. *Stroke*, [ISSN: 00392499] *39*(12), 3323–3328. http://dx.doi.org/10.1161/STROKEAHA.108.516112.

Zhang, Y., Brady, M., & Smith, S. (2001). Segmentation of brain MR images through a hidden Markov random field model and the expectation-maximization algorithm. *IEEE Transactions on Medical Imaging*, [ISSN: 02780062] *20*(1), 45–57. http://dx.doi.org/10.1109/42.906424.

Zhang, Y.-D., Hou, X.-X., Chen, Y., Chen, H., Yang, M., Yang, J., & Wang, S.-H. (2018). Voxelwise detection of cerebral microbleed in CADASIL patients by leaky rectified linear unit and early stopping. *Multimedia Tools and Applications*, *77*(17), 21825–21845. http://dx.doi.org/10.1007/s11042-017-4383-9, ISSN: 1380-7501, 1573-7721.

Zhang, Y.-D., Hou, X.-X., Lv, Y.-D., Chen, H., Zhang, Y., & Wang, S.-H. (2016). Sparse autoencoder based deep neural network for voxelwise detection of cerebral microbleed. In *2016 IEEE 22nd international conference on parallel and distributed systems (ICPADS)* (pp. 1229–1232). IEEE, ISBN: 978-1-5090-4457-3, http://dx.doi.org/10.1109/ICPADS.2016.0166.

Zhang, Y.-D., Zhang, Y., Hou, X.-X., Chen, H., & Wang, S.-H. (2018). Seven-layer deep neural network based on sparse autoencoder for voxelwise detection of cerebral microbleed. *Multimedia Tools and Applications*, *77*(9), 10521–10538. http://dx.doi.org/10.1007/s11042-017-4554-8, ISSN: 1380-7501, 1573-7721.